**1.2**

# Annual Meteorological Modeling in Support of Visibility Improvement in the Southeast US

Donald T. Olerud, Jr.* and Aaron P. Sims
Baron Advanced Meteorological Systems, Raleigh, NC

Michael Abraczinskas
North Carolina Department of Air Quality, Raleigh, NC

## 1. INTRODUCTION

In order to ultimately improve visibility in the southeastern US, the Visibility Improvement State and Tribal Association of the Southeast (VISTAS) (http://www.vistas-sesarm.org/) is in the midst of an extensive modeling effort. A 12-month modeling period is deemed necessary to cover an adequate range of visibility impairment. The meteorological component of the modeling is performed by Baron Advanced Meteorological Systems (BAMS) using the PSU/NCAR mesoscale model (MM5), (http://www.mmm.ucar.edu/mm5/mm5-home.html). This document evaluates and documents the results of that modeling.

A great deal of effort was expended to determine the optimal MM5 configuration to be implemented for the annual run. The modeling protocol (Olerud, 2003a), (http://www.baronams.com/projects/VISTAS/reports/VISTAS_TASK3a_draft.pdf) examines these sensitivity tests in detail before offering the desired model configuration and evaluation/presentation methodologies. The reader is referred to that document for the details of model implementation

## 2. DESCRIPTION OF THE METEOROLOGICAL MODELING APPROACH

The meteorological model used in this study is the PSU/NCAR Mesoscale Model (MM5 version 3.6.1+, Grell et al., 1994, MPP version), the same version of the code that was used in the sensitivity modeling. At the time the annual modeling began, the latest released version of the MM5 code was 3.6.2. Most of the v3.6.2 changes are included in the v3.6.1+ version of the code. If NCAR documentation is complete, the only modification not included involves the treatment of sea ice, a change likely to have negligible effect over the southeastern US. The v3.6.1+ code also includes an adapted version of EPA's MPP PSX code, an essential feature that does not readily port into later MM5 versions. The latest v3.6.2 MM5 preprocessors could readily be employed, so we did so. The modeling domains are shown in figure 1.

Sensitivity testing showed that the configuration that produced the most desirable results was px-acm8. This configuration is implemented for the annual run with the following physics options:

**Soil**: Pleim-Xiu land surface model
**PBL**: Asymmetric Convective Mixing
**Rad**: Rapid Radiative Transfer Model (RRTM)
**Cld**: Kain-Fritsch 2 cumulus parameterization
**Microphysics**: Reisner 1 (mixed phase)
**Analysis nudging**:
**Aloft**:
**36km**: t (2.5E-4/s), q (1.0E-5/s), u,v (2.5E-4/s)
**12km**: t (1.0E-4/s), q (1.0E-5/s), u,v (1.0E-4/s)
**Surface**:
**36km**: u, v (2.5E-4/s), T and q not nudged
**12km**: u, v (1.0E-4/s), T and q not nudged
**Observational nudging**: Not used
**Snow effects**: Turned on via IFSNOW = 1
**SST**: EDAS 24-hr averaged skin temperatures

Note that the decision to use sea surface temperatures (SST's) derived from the EDAS skin temperatures was not an arbitrary one. At the time this modeling effort began, most of the other RPO's were planning to use NCEP SST's to avoid problems that might arise from applying skin temperatures as SST's. The 1996 annual modeling effort conducted by Olerud *et al* (2000) suffered from very high inland lake temperatures as the MM5 system erroneously applied land skin temperatures to areas such as the Great Salt Lake. Fortunately the 3.6.2 version of the MM5 preprocessor INTERPF treats skin temperatures in a more appropriate manner, forcing a 24-hour average of skin temperatures if they are being used as a surrogate for SST's. The downside of using the NCEP SST fields is that they have a very coarse resolution of 2.5x2.5 degrees (~270x270 km). Alternatively the EDAS fields are available at 40-km resolution. Figures 2 and 3 show the resultant ground temperatures (equivalent to SST's over water) a few hours into test runs using the alternate

* *Corresponding author address*: Donald T. Olerud, Jr., Research Scientist, Baron Advanced Meteorological Systems, c.o. NCSU-Marine Earth and Atmospheric Sciences Dept, 1125 Jordan Hall, Raleigh, NC, 27695 don.olerud@baronams.com

SST initializations. The differences between the two approaches are clearly seen in the Gulf of Mexico. Note how appropriately warm the SST's are along the Mexican coast in the EDAS run, while the NCEP run is markedly colder and more "blocky". Similar improvements are seen in the Great Lakes and in the Gulf of California. Overall the EDAS approach seems to be the better approach.

The time-varying preprocessing is performed in six-day chunks (starting at 00Z) using fields created by TERRAIN using the "BotSoil" option from the input ~4km terrain databases. The EDAS analyses files are processed through pregrid and mapped to the MM5 grids via regridder. The fields are "improved" in LITTLE_R by incorporating the surface, ship, and upper air observations that are available from NCAR. The LITTLE_R output fields are then interpolated to the MM5 sigma coordinates by INTERPF. MM5 itself is run in 5.5-day segments with a 12-hr overlap from segment to segment. In order to allow sufficient spin-up time for subsequent air quality runs, the modeling initiated at 00Z Dec 17, 2001, continuing through 12Z Jan 1, 2003. With the exception of TERRAIN (which was executed on an SGI machine), MM5 and all its preprocessors/postprocessors were run on a 2.8GHz Xeon Linux cluster, with the core model run on 32 processors via MPP. Complete details regarding model setup and implementation, including namelist examples, are available in the aforementioned modeling protocol.

## 3. RESULTS

### 3.1 *Temperature*

Figure 4 shows the observing sites used in this model evaluation, color-coded by RPO region. Generally speaking, we use horizontal bilinear interpolation to estimate model values at the observing sites. Unlike many evaluation studies, we also address the elevation differences that often exist between the model terrain and the observational sites. If this difference exceeds 500 m, we exclude the model/obs pair from the evaluation. Otherwise, we implement a standard atmospheric lapse rate to account for the pressure-induced temperature variations that result from the elevation differences. In mountainous terrain this effect can be significant (figure 5), since observational sites are disproportionately placed in valleys.

To begin our temperature evaluation, we focus on the VISTAS region, cleanly comparing results at the 36-km and 12-km resolutions. For a description of the statistical metrics shown below, the reader is referred to Olerud (2003b), available at http://www.baronams.com/projects/VISTAS/reports/VISTAS_TASK1.pdf.

Figure 6 shows how monthly temperature biases vary throughout 2002. Note that biases are generally small, never exceeding +/- 0.8C. Nonetheless the model shows a clear predilection towards being too cold in the winter months, and the problem is exacerbated at 12-km. Presumably the increased temperature nudging strength aloft (2.5 E-4/s vs. 1.0 E-4/s) enables the coarser grid to be slightly less biased. Model biases for the May-August period are practically 0.0 at both resolutions. The seasonal aggregation of temperature biases quantifies the same result in a bar chart (figure 7).

To examine the temperature biases in greater detail, consider the day (12Z-23Z) and night (00Z-11Z) bias traces for the 12-km grid in figure 8. Clearly model performance for the daytime period is the primary reason for the wintertime cold bias. The daytime cold bias is persistent from month to month, but in the summer the model is only relatively weakly biased. The nighttime trace reveals that over the entire year the model is unbiased, being slightly low biased in the winter and slightly warm biased in the summer. There could be at least four physical mechanisms that could lead to a daytime cold bias: 1) Too cold soil initial conditions, 2) Too moist soil initial conditions, 3) Too many daytime clouds, and 4) Poor treatment of snow related processes. Once we examine the full suite of summary statistical products we will have a better idea of what is really going on. In the grand scheme of things the model temperature performance appears to be line with what we expect given the state of the art in MM5 applications. Figure 9 indicates similar temperature biases for the VISTAS region at 36-km resolution, though the magnitude of the wintertime biases are damped.

Spatial analysis (not shown) of the January 2002 aggregate temperature biases within the 12-km domain reveals that the cold bias is widespread. Most of the sites in the VISTAS states display the cold bias, but the biases are definitely larger for sites in the northern VISTAS states, especially so for sites in western NC and VA. Given the significant snowfall that fell in this area early in the month, it seems likely that less than optimum treatment of snow/snow melt might contribute to the cold biases.

To complete our statistical analyses of temperature, we have included a series of "Bakergrams" in figures 10-11 for the 12-km VISTAS region. These images place daily statistics into a tile plot in a calendar-like layout. In this way we can effectively summarize performance for the entire year in one plot. Figure 10 shows the temperature bias Bakergram. Note how small the biases are in the summer, while the wintertime cold biases are easily seen. The temperature errors

(figure 11) are also greatest in the winter. An index of agreement Bakergram (not shown) indicates that the model skill in predicting temperature is fairly high every day of the year.

### 3.2 *Mixing Ratio*

Figure 12 shows the mixing ratio bias trace over for 2002 for both model resolutions for the VISTAS region. The model exhibits a slight positive bias in January, especially at 36-km resolution. Considering that the average observed mixing ratio in January is on the order of 4 g/kg, this bias is more significant that an equivalent bias in July, when average observed mixing ratios are on the order of 15 g/kg. Might this positive moisture bias be the root cause of the temperature cold bias? Probably not, since the cold bias was larger in the 12-km grid, not the 36-km grid where the moisture bias is more significant.

Another striking observation about the mixing ratio bias traces is the low biases noted in the fall months, shown well in figure 13. These values easily fall within the benchmark expectation of +- 1.0 g/kg, but it is curious that the model shows that signature. Figures 14-15 show that the model is systemically dry-biased during the afternoon for non-winter months. Usually one associates such a feature with too much mixing (or too efficient mixing) in the model, thus bringing dry air from aloft to the surface. For most of the year the model is slightly moist biased at night, but in the fall the night shows a slight dry bias. The combination leads to the overall dry bias noted for that season. Site-specific moisture biases (not shown) for September over the 12-km grid were created. They indicate that the sites in Virginia and western North Carolina show the largest dry bias, while many areas (eastern NC, northern FL, MI) show a moist bias. Such spatial discrepancies in model performance over small areas suggest that either the model is failing to capture smaller-scale variations properly, or that the model is introducing smaller-scale variations where none exist. One of the striking differences between eastern North Carolina (moist bias) and western North Carolina (dry bias) is the soil types prevalent in those areas. Perhaps there are issues with the soil moisture/temperature initializations that lead to the performance differences over small areas? Figure 16 shows the September "Bakergram" for moisture bias over the 12-km VISTAS region. These plots display hourly biases in a tile plot format, with the day of the month increasing from left to right, and the UTC hour of the day increasing from top to bottom. Recall that the model is run in 5-day segments such that every fifth day at 13Z results from a new segment are introduced. The first new segment in September starts on the 3rd. Moisture biases tend to significantly worse at the beginning of a segment than they are at the end of a segment, indicating that there does indeed seem to be soil initialization issues that are affecting the model.

The annual Bakergrams for mixing ratio (figures 17-18) clearly indicate the autumn dry bias. Because mixing ratio nonlinearly increases with temperature, larger errors are found in the summer. The most disconcerting mixing ratio statistic is the fall dry bias, even though the absolute errors are lower in the fall than in the summer.

### 3.3 *Relative Humidity*

With the January cold/dry bias, we would expect that relative humidity would be high biased. Figure 19 indicates that is indeed the case. Generally, however, relative humidity is unbiased. The fall dry bias noted above does result in a low RH bias (figure 20) that is especially noticeable in November. The model tends to be positively biased during the daytime and negatively biased at night (figure 21). Spatially (not shown) the model is actually slightly high biased just north of the VISTAS states, but the heart of the region from Virginia to Mississippi is biased low. The November relative humidity bias Bakergram (figure 22) shows some segment initialization signatures, but not as decisively as was seen in the mixing ratio September Bakergram (figure 16). Completing our suite of relative humidity plots are the annual Bakergrams (figures 23-24).

### 3.4 *Wind Speed*

Let us now focus on wind speed performance, starting with the standard include-all-calms-as-zero approach. Figure 25 shows that the model is positively biased with regard to wind speed for all months and for both grids. The bias is especially acute at 12-km resolution, presumably due to the weaker nudging applied to the winds at that scale. The greatest bias occurs in November, while the smallest bias occurs in March. Both are surprising results. The seasonal bar chart (figure 26) shows a general increase in speed bias from spring to autumn. Figures 27-28 reveal that the bulk of the speed bias occurs at night, quite likely in part to the presence of numerous calm observations. The site-specific spatial bias plot for this month (not shown) reveals that the northern third of the region is generally unbiased with regard to wind speed, while most of the VISTAS states exhibit a weak to moderate positive bias, peaking in North Carolina. Figure 29 shows that the speed biases are indeed primarily nighttime phenomena, and demonstrate that weak wind speeds lasting almost the entire day is not uncommon in the southeast. The annual wind speed Bakergrams are shown in figures 30-31.

So what happens statistically if we consider only non-zero wind speed observations? Figure 32 shows that the resultant biases are practically non-existent at 12-km, while a slight low bias is evidenced at 36-km. Figure 33 consolidates the

data into seasonal bins. So clearly the majority of the wind speed (regular) high biases stem from comparing model winds, which have no threshold issues, with observations, which obviously do. Figures 34-35 break the data into day/night periods.

We have already discussed how not including calm reports probably introduces a low bias into the wind speed calculations. Figures 36-38 show the results we obtain by substituting a value of 1.5 knots (mid-point between 0.0 and lowest observed report of 3 knots) for each of the calm reports. A general positive bias is noted, especially at night and at 12-km resolution, but the magnitude of the biases are reduced by ~0.2 m/s.

### 3.5 *Wind Direction*

Let us now consider wind direction performance. Figure 39 shows the monthly wind direction errors over the VISTAS region for both model domains. The performance of the two grids is very similar, and surprisingly enough the 12-km grid has a slightly lower error. The increased nudging strength at 36-km might have been expected to yield a lower direction error. We know that all wind direction errors do not have the same effect of air quality modeling. A 90 degree direction error at light winds speeds might have a less deleterious effect than a 40 degree error at moderate wind speeds. A better way of treating wind direction discrepancies between the model and the observations is to calculate the magnitude of the error wind vector. This approach properly treats winds as vectors and allows us to quantify the combined effect of speed and direction errors. Figure 40 shows the resultant plot. As a rule the two grids track very similarly, with the 36-km domain yielding slightly superior results, undoubtedly due to the presence of stronger nudging. Also note how the result for November does not stick out as an outlier, even though wind speed performance exhibited its highest bias during that month. The wind direction bias and error annual Bakergram plots are displayed in figures 41-42, followed by the annual Bakergram for the magnitude of the error wind vector in figure 43.

### 3.6 *Clouds*

Since the alternative cloud fraction variable "CLD2" is deemed more meteorologically consistent with the cloud observations than is the MCIP-derived variable "CLD", we will focus our attention there. Figures 44-45 show a strong seasonal variation to cloud bias. For most of the year clouds are relatively unbiased. However, through the summer months a noticeable positive bias appears, especially at 12-km. Figures 46-47 show that most of the bias occurs at night. It is difficult to know if this nighttime bias is indeed real, since cloud observations at night might not be as accurate as they are during the daytime. A spatial statistical plot (not shown) indicates that the bias for July is widespread with little spatial variation. The Bakergram (figure 48) reveals that the nighttime bias is more or less a constant feature. If the observations are accurate, it appears that MM5 is lacking a key cloud disintegration process that occurs in the real world. Figures 49-50 show the average observed and modeled cloud coverage in a Bakergram format. Note that the observations show a distinct diurnal variation in that cloud coverage is greatest in the afternoon and smallest in the late overnight periods. Another evident cycle occurs at the synoptic scale and can be seen on an approximately 10-day time scale. The model does a nice job replicating the synoptic scale variations, but the diurnal variations are completely out of phase. Since the nocturnal bias is more significant at 12-km than it is at 36-km, one must consider the possibility that the internal cloud parameterizations need to be adjusted to run as successfully at finer scale resolutions. The annual bias and error Bakergram products for clouds are shown in figures 51-52.

### 3.7 *Precipitation*

To begin our precipitation analysis, consider the monthly obs/model accumulated precipitation plot for the 12-km grid for January (figures 53). Note the nice job the does in replicating the observed precipitation field. However, the model appears to noticeably overestimate the amount of precipitation in the summer months, especially in July (figure 54). Interestingly enough in the fall the model underestimates precipitation amounts (not shown), coinciding with the dry bias noted in the mixing ratio statistics (figure 13).

The summertime accumulation bias could result from at least two model inadequacies. One is that the model could fire off convection (or just regular rain for that matter) too often, possibly most every afternoon. The second possibility is that the model triggers rainfall at approximately the correct frequency, but the model could overestimate the intensity of the rainfall. The first possibility is the more serious model flaw from an air quality perspective, since the presence/absence of rain affects pollution concentrations more than predicting 2 inches of rain when only 1 inch actually occurred. To address this issue, consider the statistical time series plots for precipitation shown in figures 55-60. Figure 55 shows the precipitation statistics for the 0.01-inch threshold level at 12-km resolution, and reveals that the model is slightly biased high for the first third of the year. During the summer the model is slightly low biased, reaching a yearlong minimum in September. By December the model has essentially become unbiased. When examining these statistical plots, remember that the process of gridding observed precipitation could cause the spatial extent of precipitation coverage – especially

at lower thresholds - to be slightly larger than what it really is. This would introduce an artificial negative precipitation bias. At the same time, we are assuming that any precipitation that falls in a cell covers the entire cell, which may or may not be true. This effect could cause an artificial high precipitation bias. With those caveats out of the way, it is interesting that the precipitation bias trace is similar to the mixing ratio bias trace (figure 12). The threat score indicates that the model shows considerable skill in predicting measurable precipitation year-round, with the expected slight decline in skill over the summer months. The 36-km results (figure 56) show unbiased statistics for the first half of the year, followed by a slight negative bias that maintains itself the entire second half of the year.

Figure 57 shows the 12-km precipitation statistics at the 0.05-inch threshold. The results are not all that different from the 0.01-inch threshold results, though the summertime threat scores are slightly lower. Figure 58 reveals that the 36-km precipitation (0.05-inch) is slightly biased high for the first eight months of the year, after which it becomes essentially unbiased. At the higher threshold level of 0.25-inch, figures 59-60 show that the model exhibits a significant summer increase in precipitation bias.

These statistics indicate that the model suffers from the more benign weakness mentioned above, namely overestimating the predicted amount of precipitation when it actually occurs. Perhaps the model precipitation efficiency is too great? More research needs to be made on this topic.

## 4. Summary and Conclusions

- Generally speaking, MM5 performed quite well at both 36-km and 12-km resolutions. Synoptic features were routinely accurately predicted, and the model showed considerable skill in replicating the state variables. Most of the time the model statistics easily fell within the expected “benchmarks”.

- The model shows evidence of being adversely affected by poor soil initialization at times. This is particularly evident for September and November, and it might cause the autumnal dry bias evidenced both in the mixing ratio statistics and also in the precipitation statistics. At the time of our modeling, the P-X LSM only allowed three soil initialization options: 1) Table look-up, 2) EDAS, and 3) interppx. Sensitivity testing showed that interppx can produce more severe cold biases, so we chose the EDAS option. Unfortunately that option initializes soil moisture from a layer 100-200 cm deep, whereas the P-X LSM extends downward only 100 cm. In the future improved model performance might be attained by more wisely initializing soil moisture.

- The model is noticeably cold biased in the winter months. This was expected based on our sensitivity modeling, and it appears to be related to the manner in which soil temperatures are initialized.

- The summertime diurnal cloud cycle appears to be out of phase with the observed cycle. The model maximizes cloud coverage at night and minimizes cloud coverage in the afternoon, while the observations indicate that the exact opposite should occur.

- The model noticeably overestimates the amount of summertime precipitation, but not the spatial coverage of measurable precipitation.

- While no modeling is perfect, the results of this effort should produce credible inputs for subsequent air quality modeling.


## ACKNOWLEDGEMENTS

Atmospheric data were provided by the Data Support Section of the Scientific Computing Division at the National Center for Atmospheric Research. NCAR is supported by grants from the National Science Foundation. Original sources of the datasets ds353.4, ds464.0, and ds609.2 were provided to NCAR by the National Center for Environmental Prediction. The original source of dataset ds472.0 was provided to NCAR by the Techniques Development Laboratory.

Profiler data obtained from the NOAA Profiler Network were provided by Forecast Systems Lab. Daily US .25x.25 gridded precipitation observations were provided by the Climate Prediction Center. Visible and Infrared satellite imagery were obtained from the National Climatic Data Center’s historical GOES browse server. Surface analysis maps were obtained from Unisys website, weather.unisys.com; the data on this site are provided from the National Weather Service via the NOAAPORT satellite data service.

Specific sites of surface station data for time-series plots were obtained from the National Park Service courtesy of NPS Air. These data are part of the Interagency Monitoring of Protected Visual Environments (IMPROVE) monitoring sites.

Additional surface data from the SouthEastern Aerosol Research and Characterization Study experiment (SEARCH) were obtained from Atmospheric Research and Analysis, Inc. Other surface data were provided courtesy of Mike Abraczinskas of NCDAQ.

The authors would like to acknowledge MCNC Enterprise Grid Services for the use of their computation resources. We would like to thank Kirk Baker of LADCO for his initial development of the Mosaic summary plots (Bakergrams). We also would like to acknowledge Nick Witcraft of NCDAQ for the generation and use of most of the excel plots.

**REFERENCES**

Grell, G. A., J. Dudhia, and D. R. Stauffer, 1994: A description of the fifth-generation Penn State/NCAR Mesoscale Model (MM5). NCAR Tech. Note, NCAR/TN-398+STR, 122 pp.

Olerud, D. K. Alapaty, and N. Wheeler, 2000: Meteorological Modeling of 1996 for the United States with MM5. MCNC – Environmental Programs, Research Triangle Park, NC. Final report submitted to OAPQS, US EPA.

Olerud, D. T., 2003a: Recommended MM5 Sensitivity Modeling in Support of VISTAS (Visibility Improvement - State and Tribal Association)] VISTAS Task 2b deliverable. Available from Mike Abraczinskas, Meteorologist, NC Division of Air Quality, 1641 Mail Service Center, Raleigh, NC 27699-1641

Olerud, D. T., 2003b: Evaluation Methodologies for Meteorological Modeling in Support of VISTAS (Visibility Improvement - State and Tribal Association), VISTAS task 1 deliverable. Available from Mike Abraczinskas, Meteorologist, NC Division of Air Quality, 1641 Mail Service Center, Raleigh, NC 27699-1641

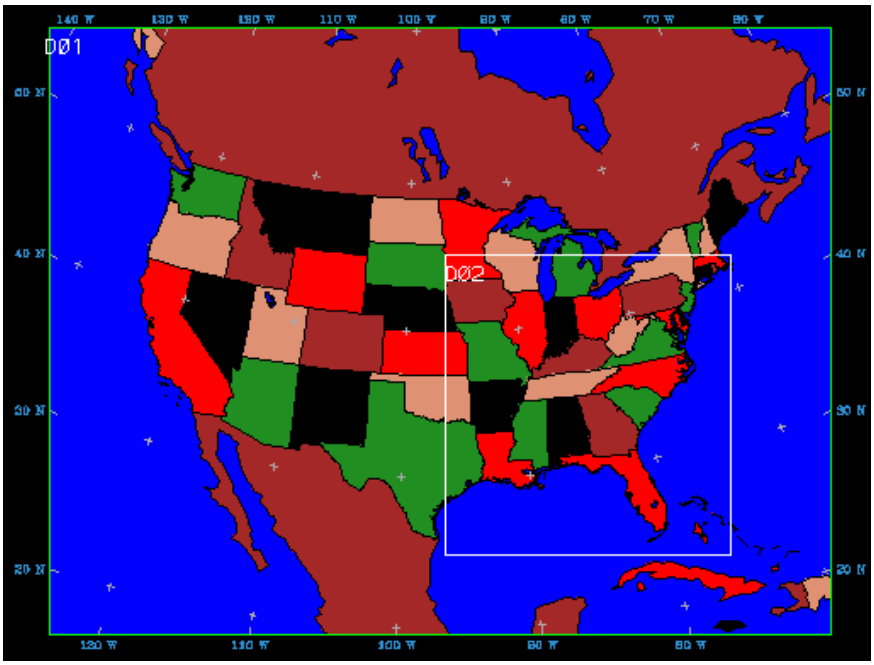


Figure 1. VISTAS 36-km/12-km MM5 modeling domain

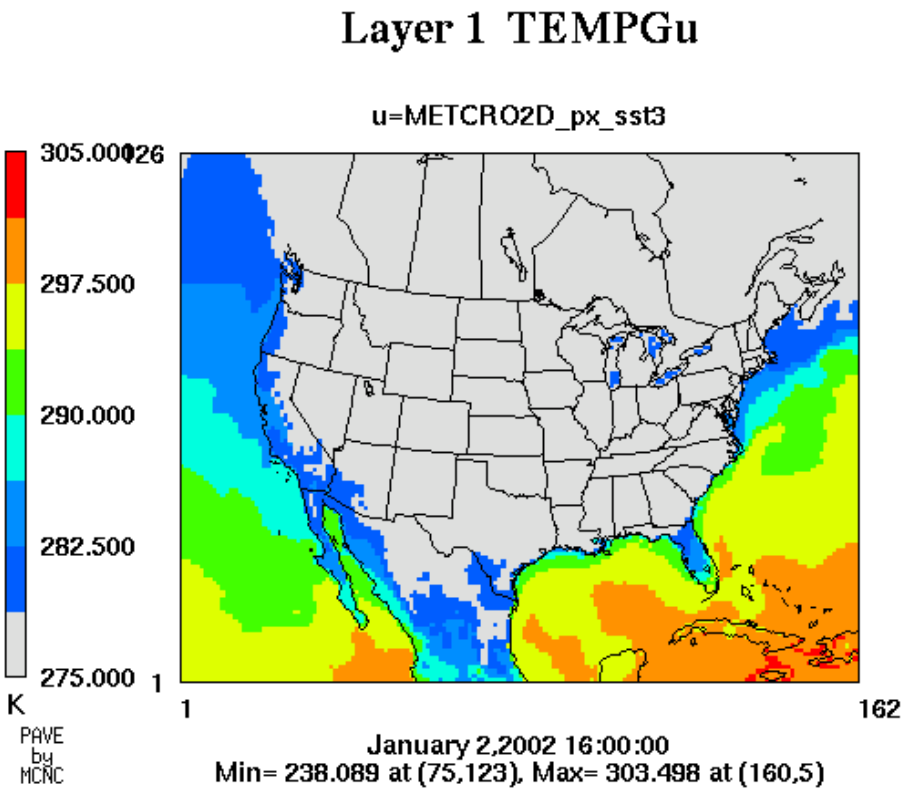


Figure 2. Ground (sea surface) temperatures resulting from an EDAS skin temperature MM5 initialization.

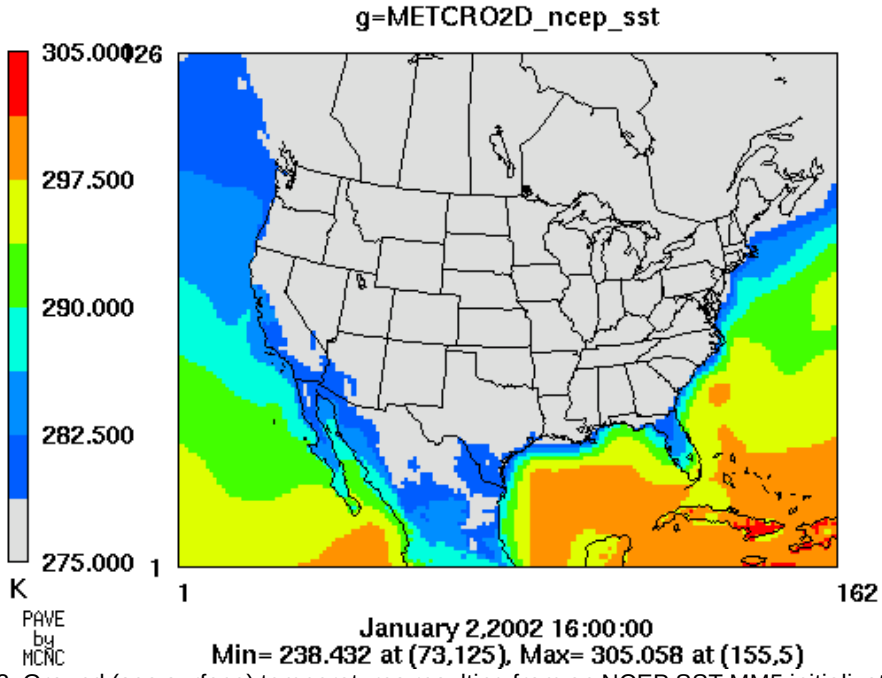

Figure 3. Ground (sea surface) temperatures resulting from an NCEP SST MM5 initialization.

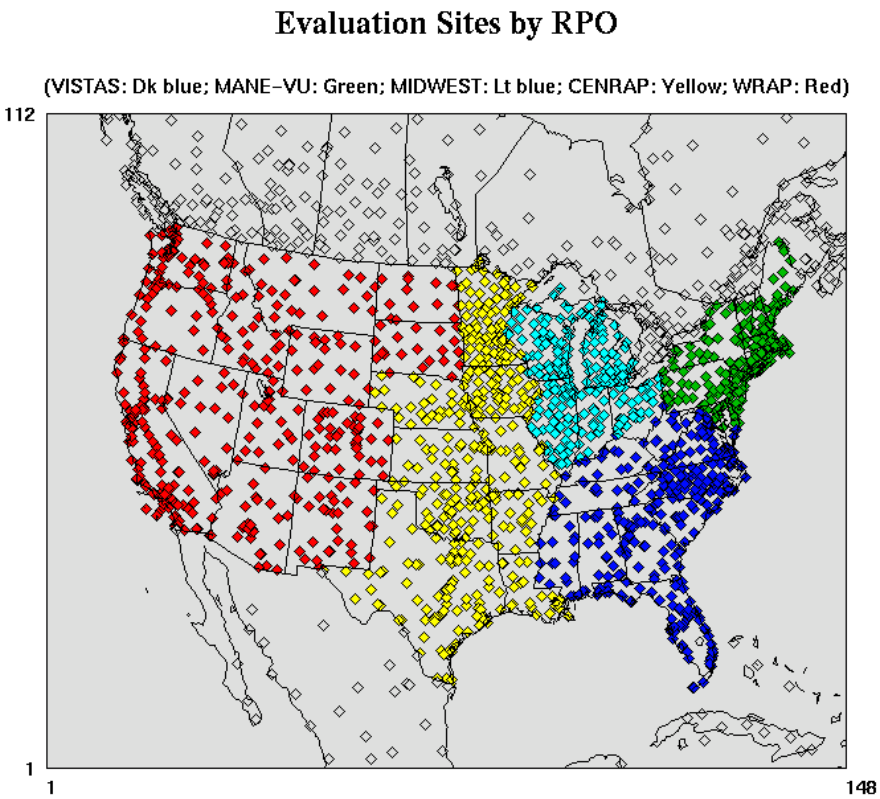

Figure 4. Surface observing network color-coded to represent Regional Planning Organization areas.

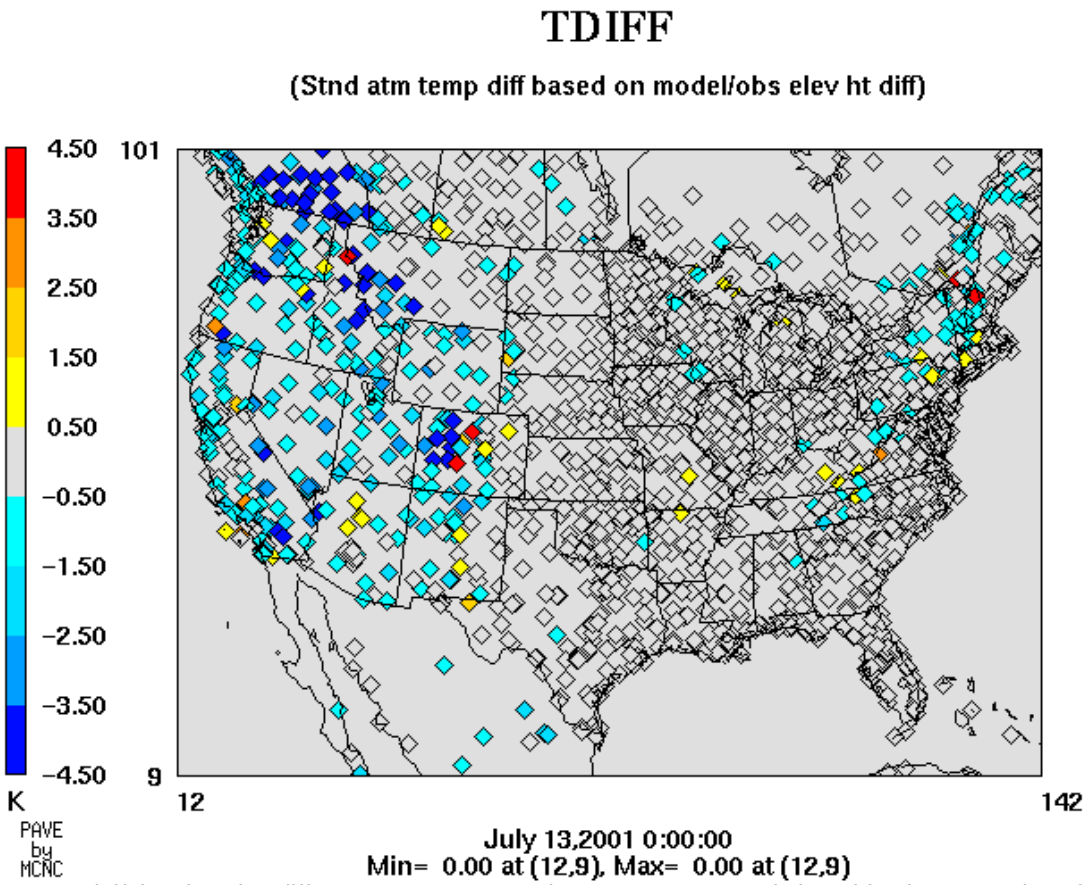


Figure 5. Model/obs elevation differences are converted to temperatures and plotted for the US portion of the 36-km grid. The temperatures are calculated assuming a standard atmosphere lapse rate of 6.5C/km, and practically indicate the temperature biases that might result solely by ignoring elevation-induced temperature effects. All of the observing sites are shown, including those sites that we ignore when calculating statistics due to their elevations being more than 500m different than the corresponding model elevations.

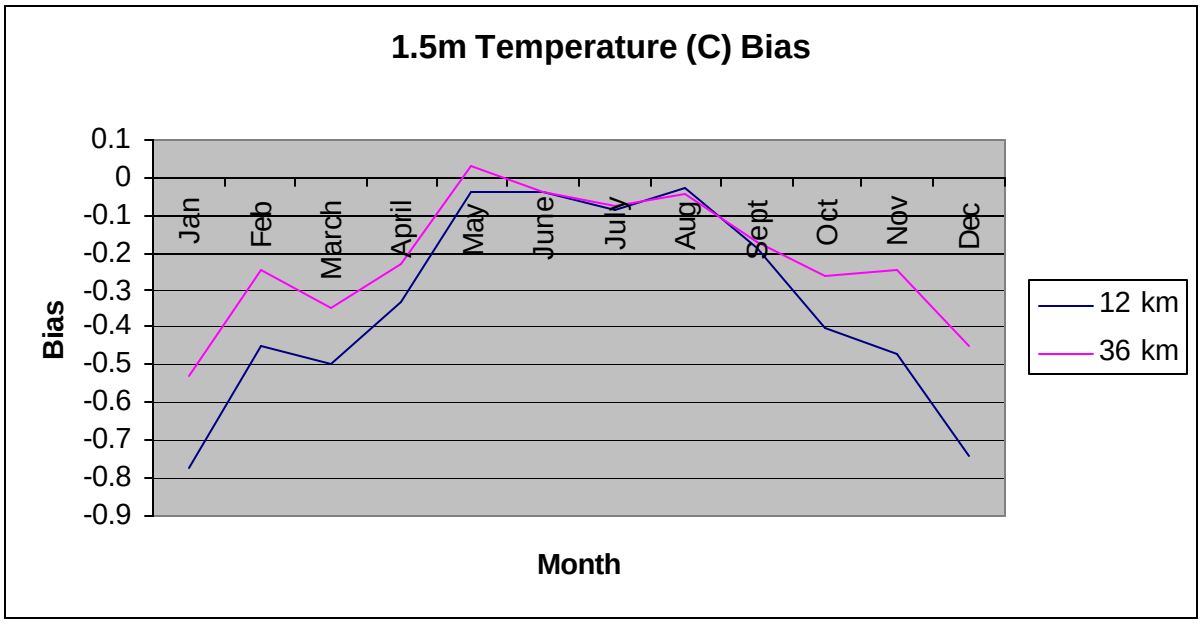


Figure 6. VISTAS region monthly temperature biases are plotted for both 12-km and 36-km resolutions.

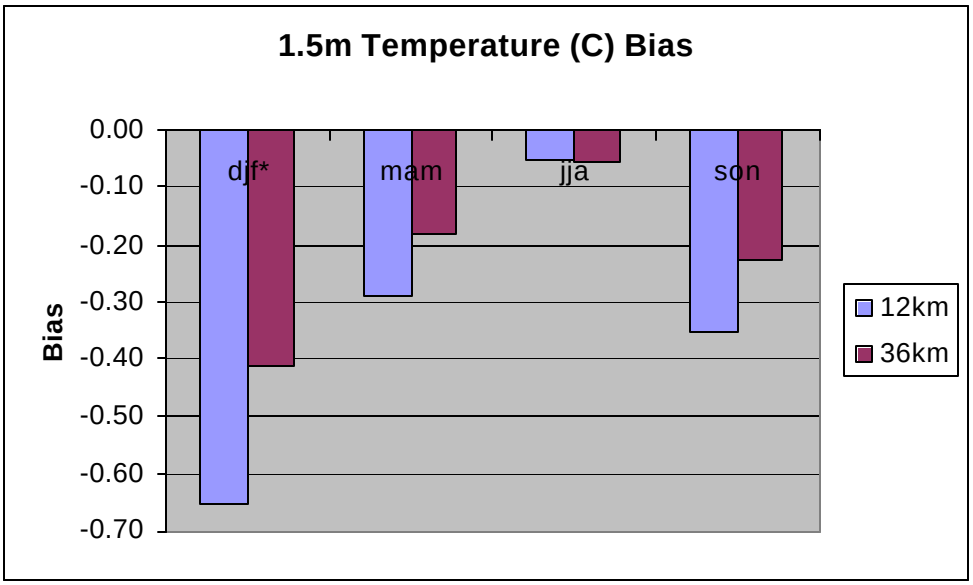


Figure 7. Seasonally aggregated VISTAS region temperature biases are shown for both the 36-km and 12-km grids.

* All months are in 2002, so the winter (djf) bar graph represents a discontinuous time period.

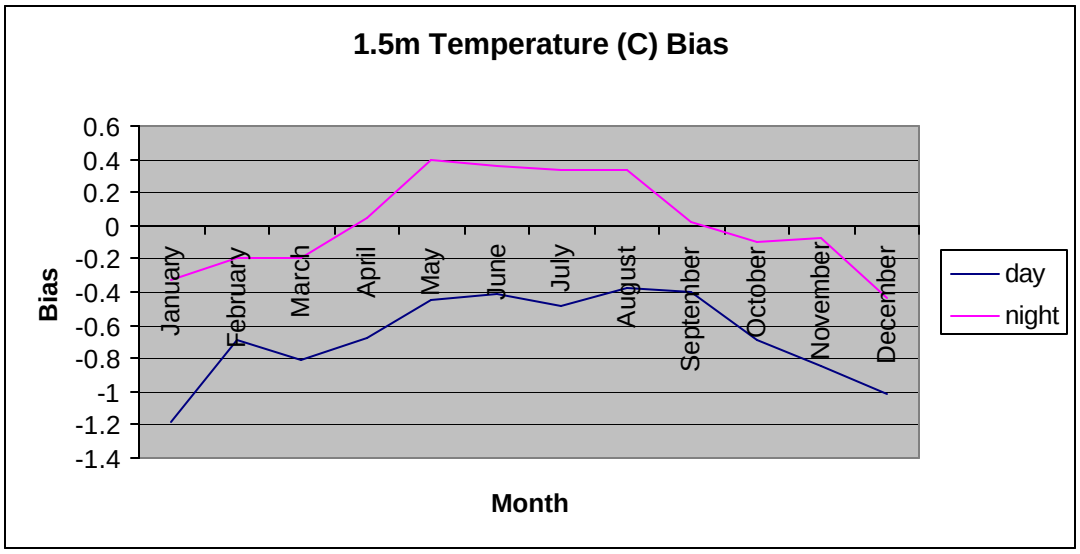


Figure 8. Monthly temperature biases for the 12-km VISTAS region are plotted. The “day” period is defined to be 12Z-23Z, while “night” is defined to be 00Z-11Z.

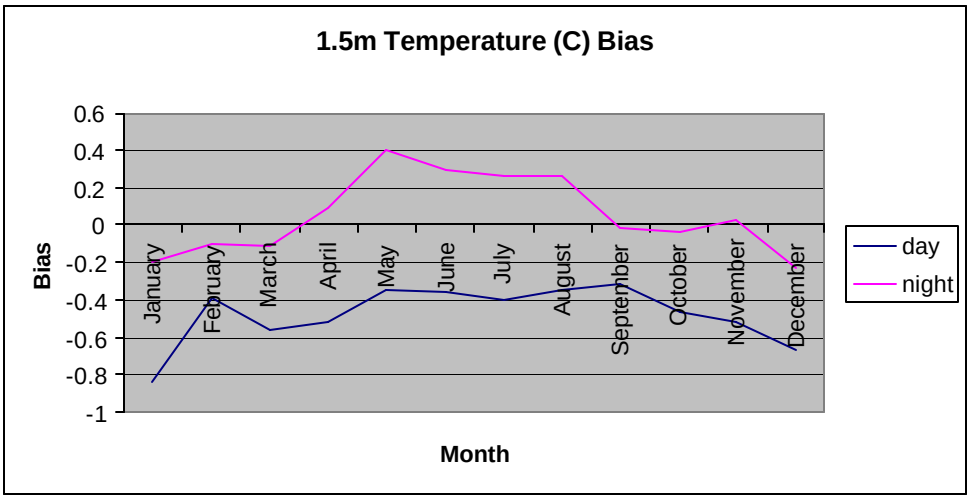


Figure 9. Monthly temperature biases for the 36-km VISTAS region are plotted. The “day” period is defined to be 12Z-23Z, while “night” is defined to be 00Z-11Z.

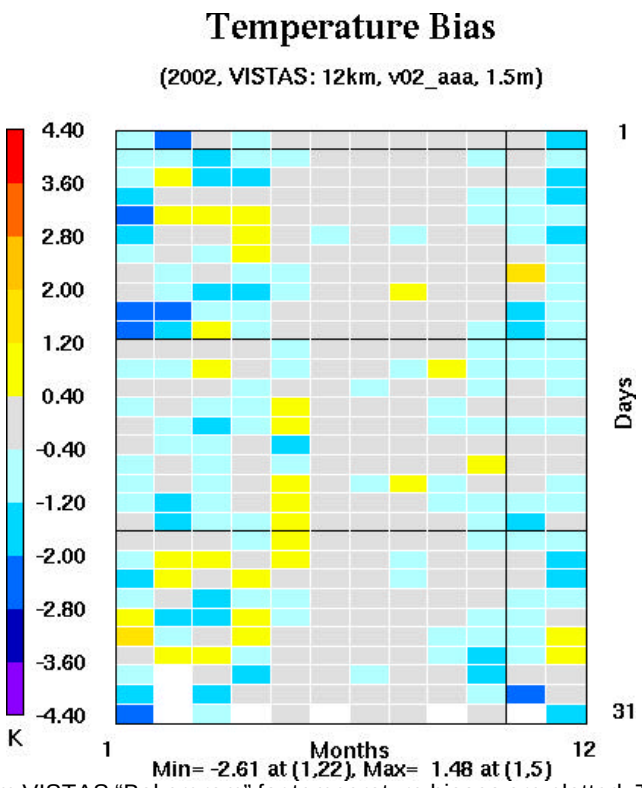


Figure 10. The 2002 12-km VISTAS "Bakergram" for temperature biases are plotted. The data are shown in a calendar-like layout so that the upper left cell represents the bias on the first day of January.

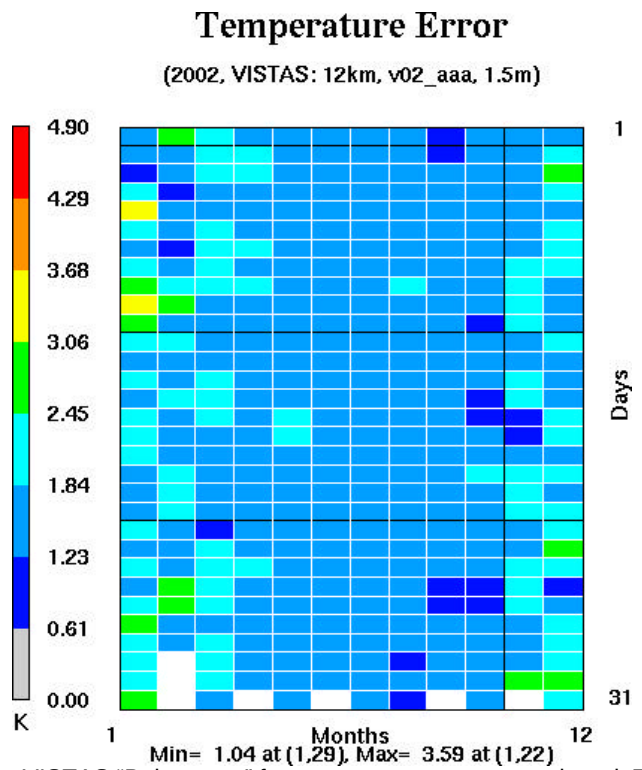


Figure 11. The 2002 12-km VISTAS "Bakergram" for temperature errors are plotted. The data are shown in a calendar-like layout so that the upper left cell represents the bias on the first day of January.

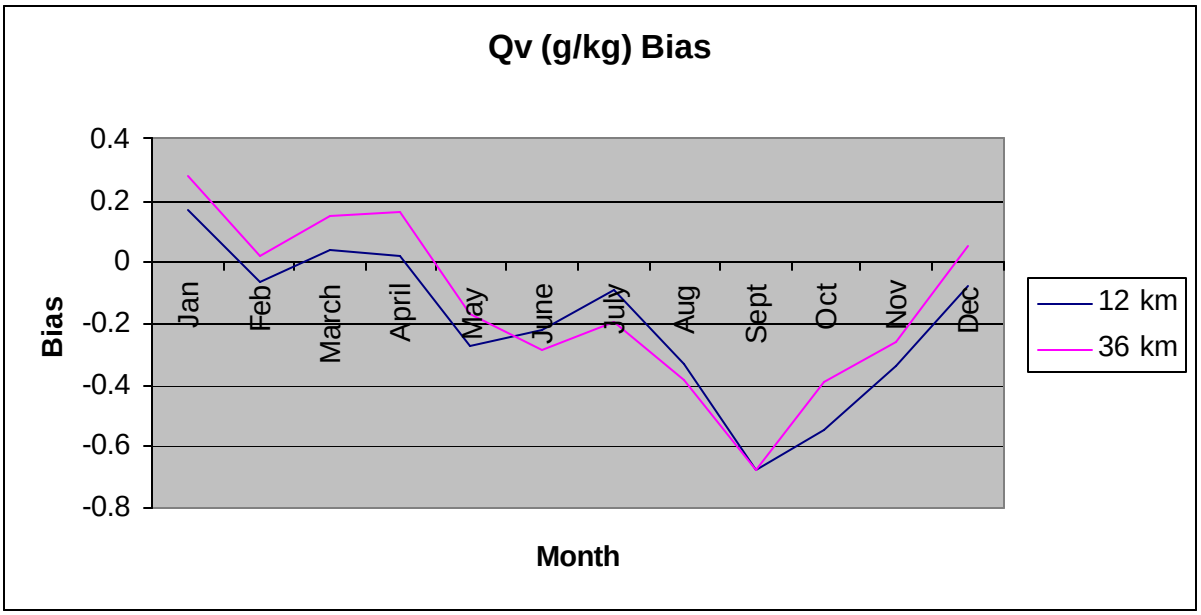


Figure 12. VISTAS region monthly mixing ratio biases are plotted for both 12-km and 36-km resolutions.

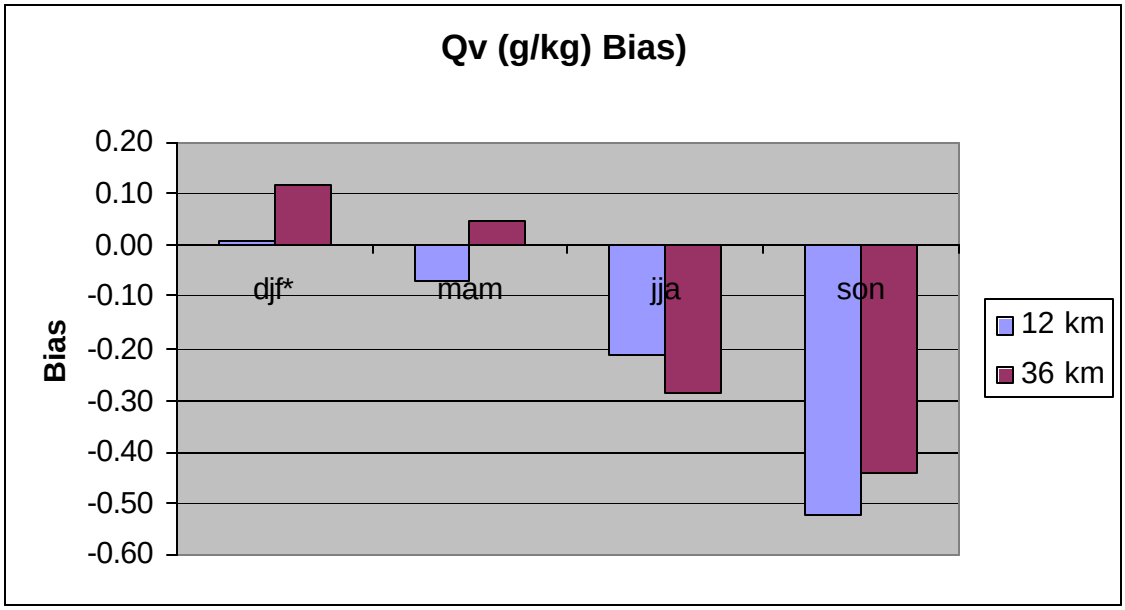


Figure 13. Seasonally aggregated VISTAS region mixing ratio biases are shown for both the 36-km and 12-km grids.

* All months are in 2002, so the winter (djf) bar graph represents a discontinuous time period.

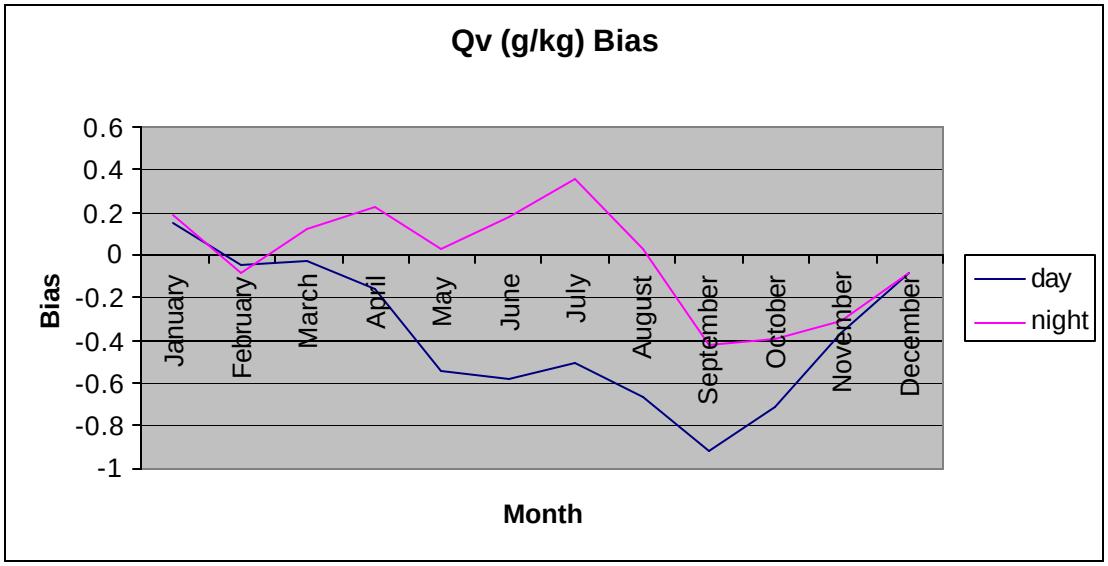


Figure 14. Monthly mixing ratio biases for the 12-km VISTAS region are plotted. The “day” period is defined to be 12Z-23Z, while “night” is defined to be 00Z-11Z.

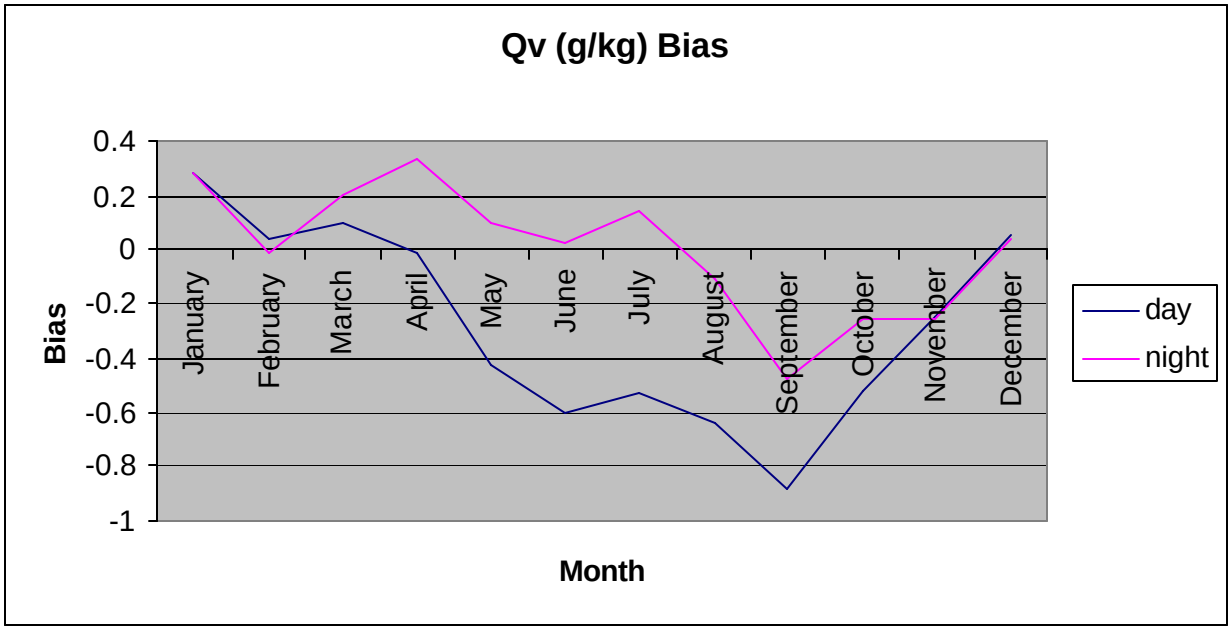


Figure 15. Monthly mixing ratio biases for the 36-km VISTAS region are plotted. The “day” period is defined to be 12Z-23Z, while “night” is defined to be 00Z-11Z.

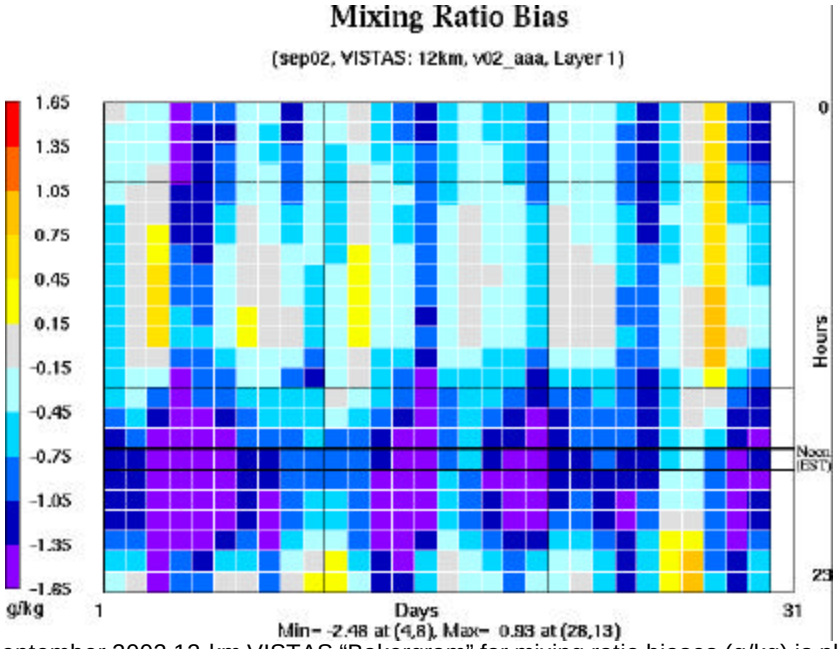


Figure 16. The September 2002 12-km VISTAS "Bakergram" for mixing ratio biases (g/kg) is plotted. The hourly biases are shown in a calendar-like layout so that the upper left cell represents the 00Z bias on the first day of the month.

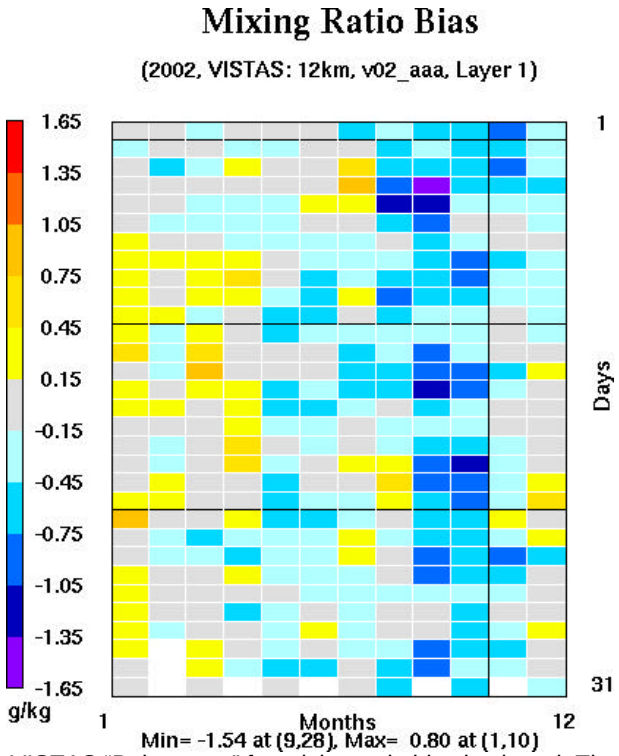


Figure 17. The 2002 12-km VISTAS "Bakergram" for mixing ratio bias is plotted. The data are shown in a calendar-like layout so that the upper left cell represents the bias on the first day of January.

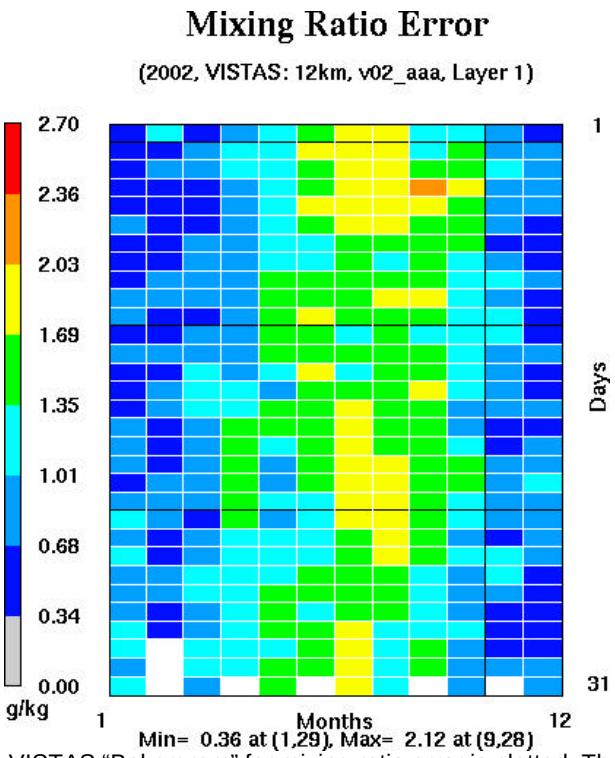


Figure 18. The 2002 12-km VISTAS "Bakergram" for mixing ratio error is plotted. The data are shown in a calendar-like layout so that the upper left cell represents the bias on the first day of January.

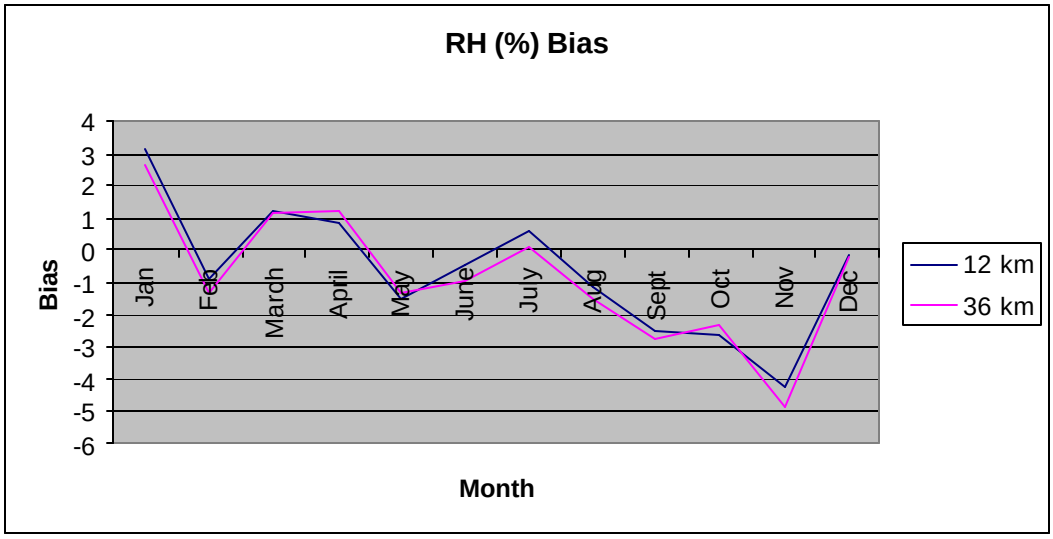


Figure 19. VISTAS region relative humidity biases (%) are plotted for both 12-km and 36-km resolutions.

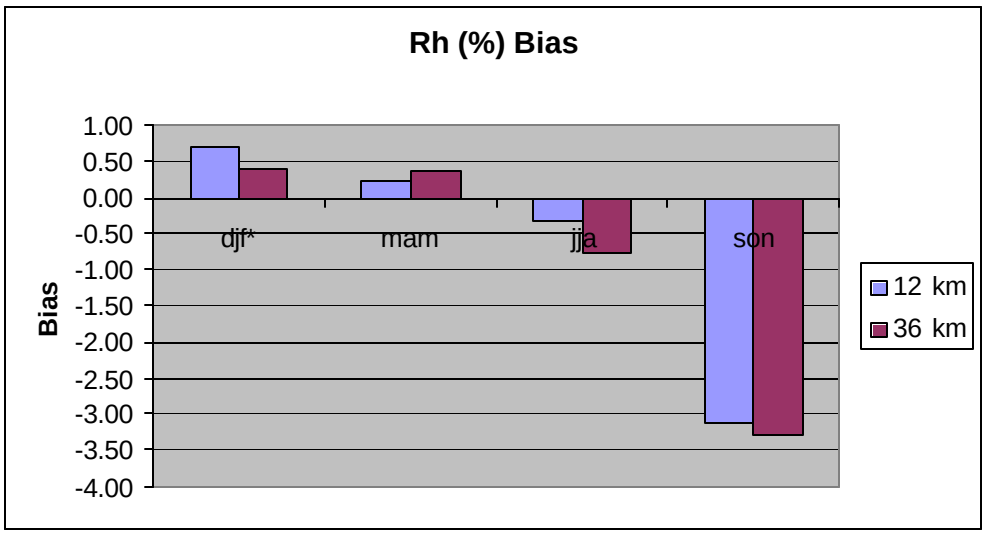


Figure 20. Seasonally aggregated VISTAS region relative humidity biases are shown. All months are in 2002, so the winter (djf) bar graph represents a discontinuous time period.

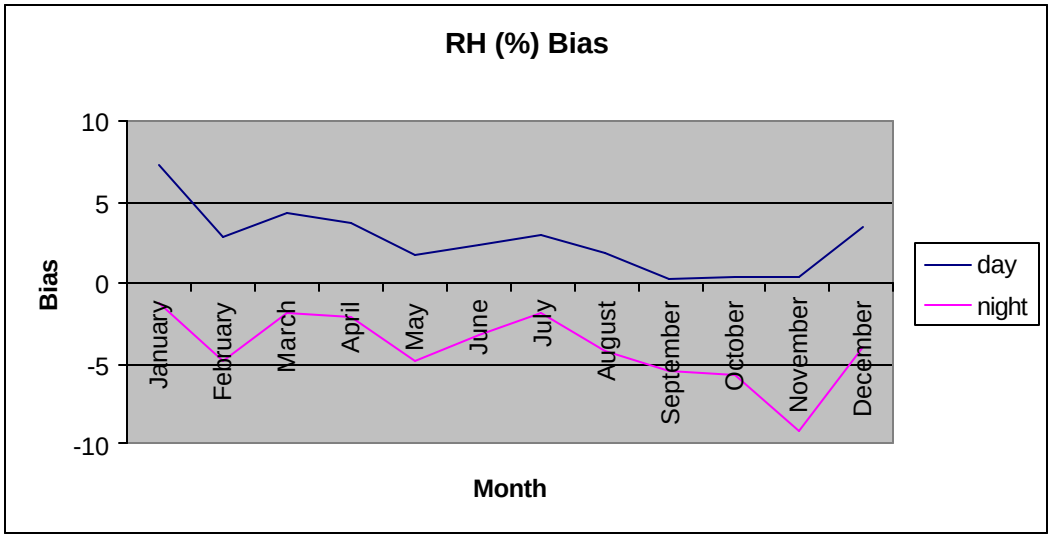


Figure 21. Monthly RH biases for the 12-km VISTAS region are plotted. The “day” period is defined to be 12Z-23Z, while “night” is defined to be 00Z-11Z.

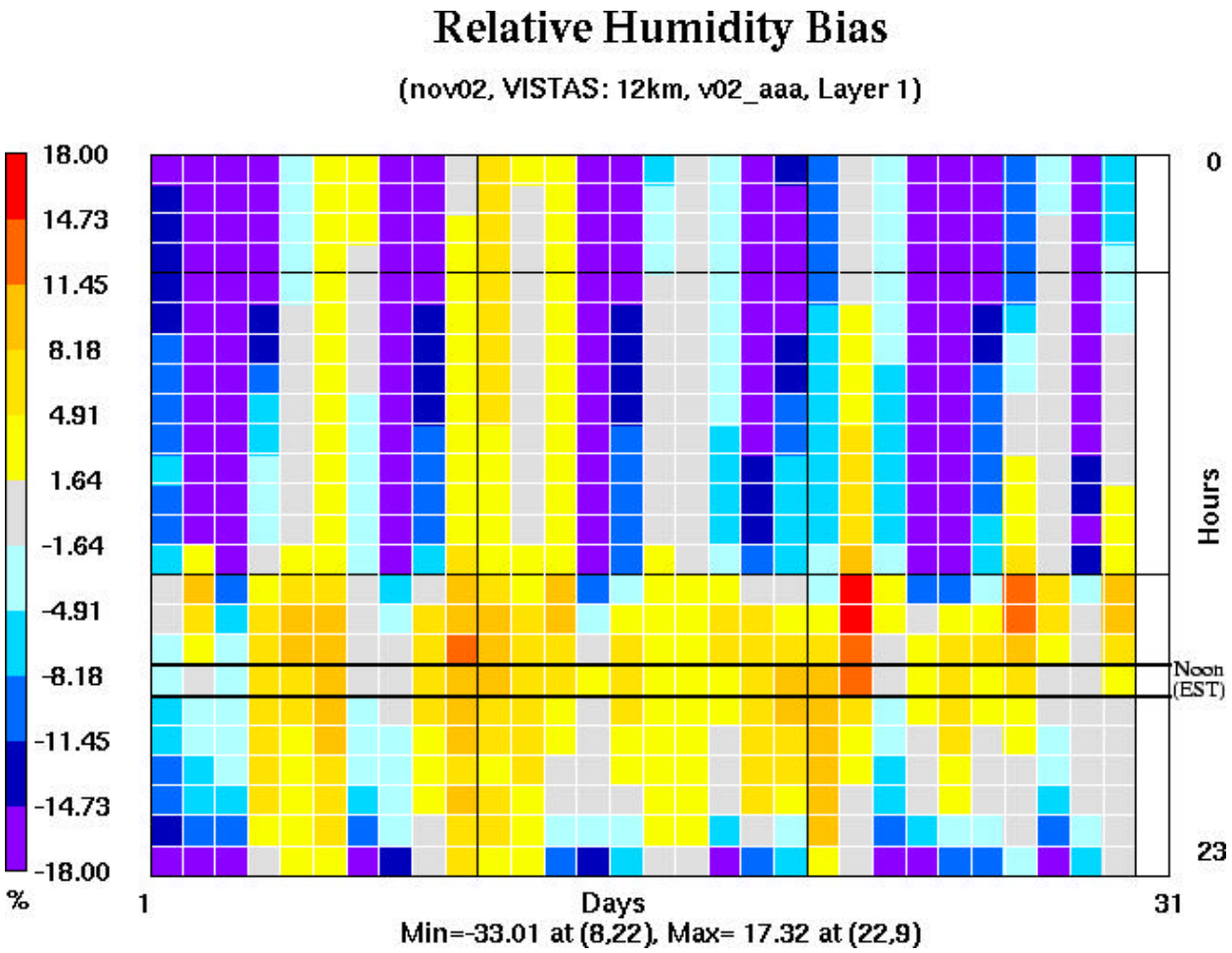


Figure 22. The November 2002 12-km VISTAS “Bakergram” for relative humidity biases (%) is plotted. The hourly biases are shown in a calendar-like layout so that the upper left cell represents the 00Z bias on the first day of the month.

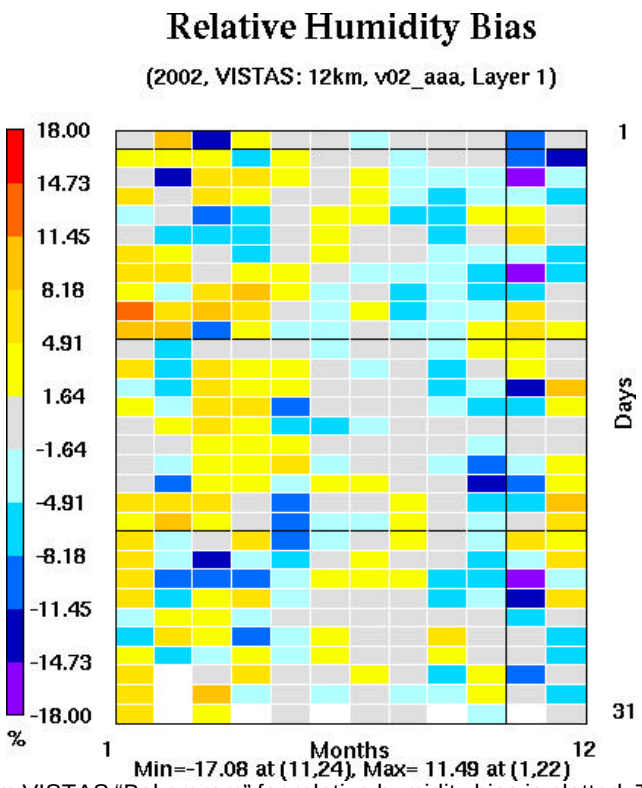


Figure 23. The 2002 12-km VISTAS "Bakergram" for relative humidity bias is plotted. The data are shown in a calendar-like layout so that the upper left cell represents the bias on the first day of January.

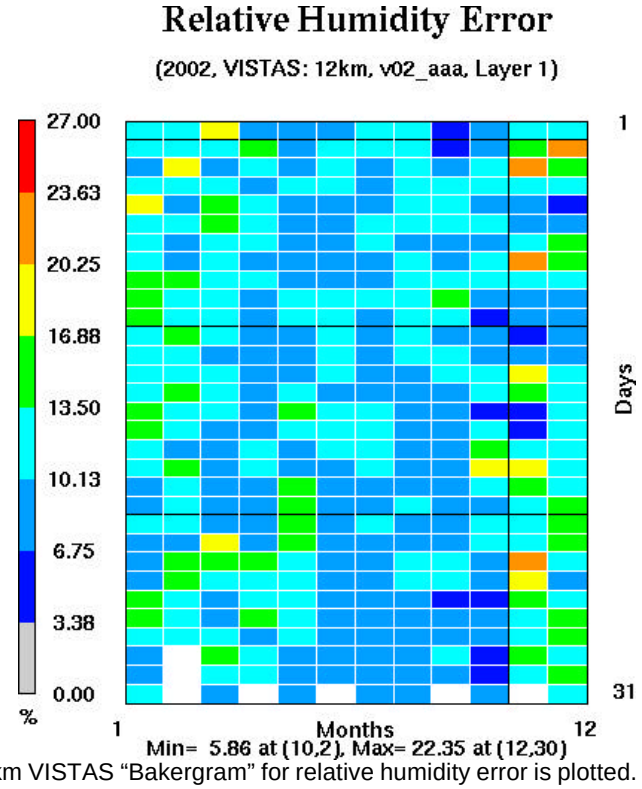


Figure 24. The 2002 12-km VISTAS "Bakergram" for relative humidity error is plotted. The data are shown in a calendar-like layout so that the upper left cell represents the bias on the first day of January.

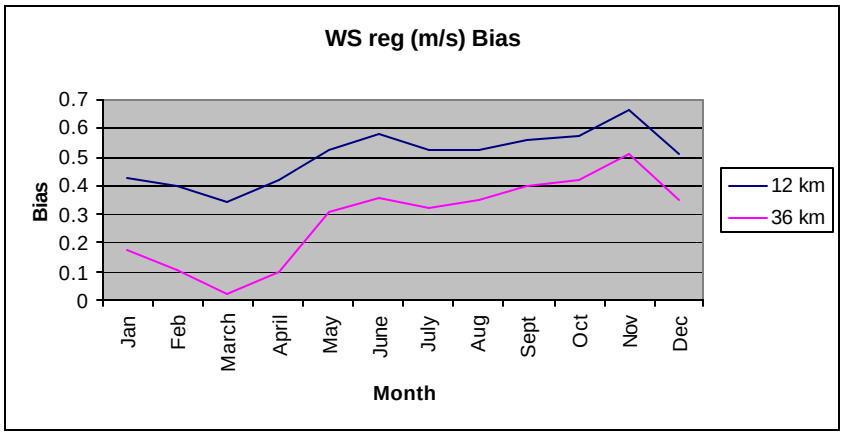


Figure 25. VISTAS region wind speed (regular) biases (m/s) are plotted for both 12-km and 36-km resolutions.

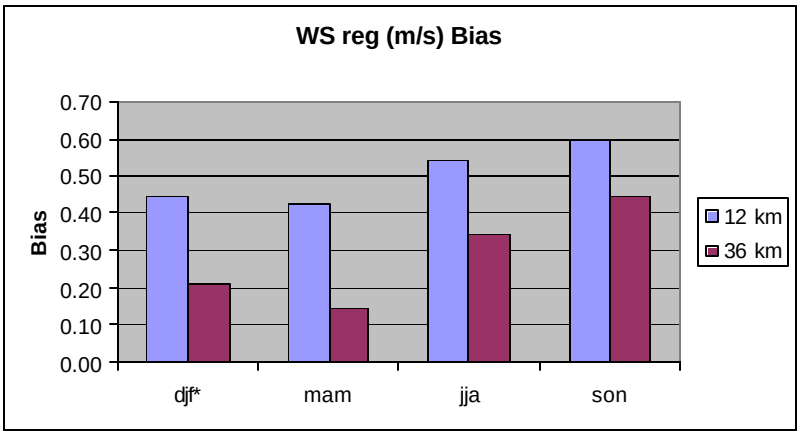


Figure 26. Seasonally aggregated VISTAS region wind speed (regular) biases are shown for both the 36-km and 12-km grids.

*All months are in 2002, so the winter (djf) bar graph represents a discontinuous time period.

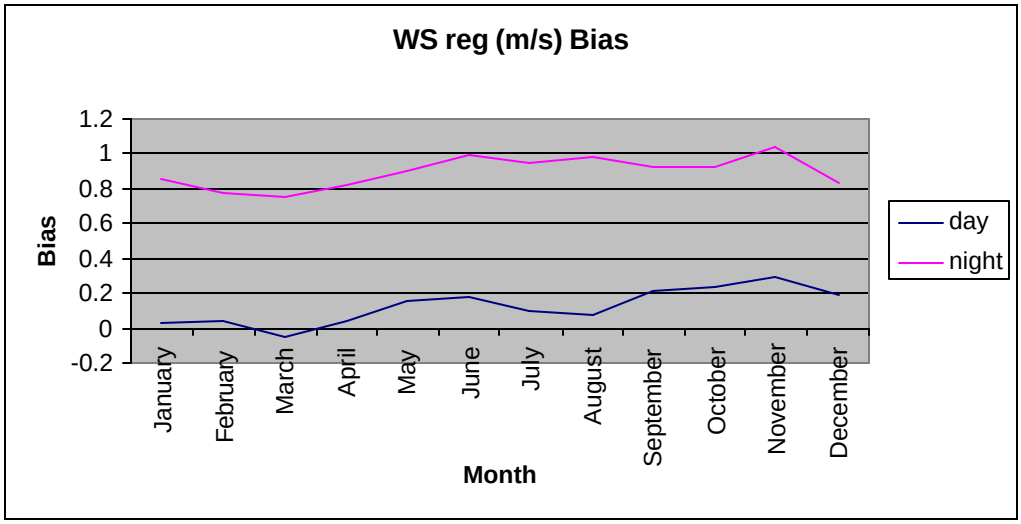


Figure 27. Monthly wind speed (regular) biases for the 12-km VISTAS region are plotted. The “day” period is defined to be 12Z-23Z, while “night” is defined to be 00Z-11Z.

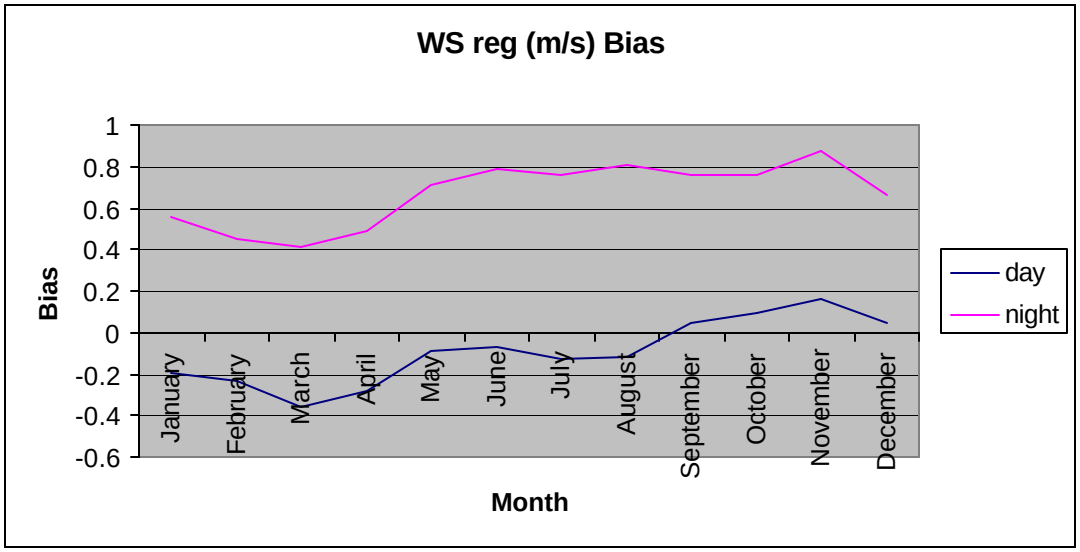


Figure 28. Monthly wind speed (regular) biases for the 36-km VISTAS region are plotted. The “day” period is defined to be 12Z-23Z, while “night” is defined to be 00Z-11Z.

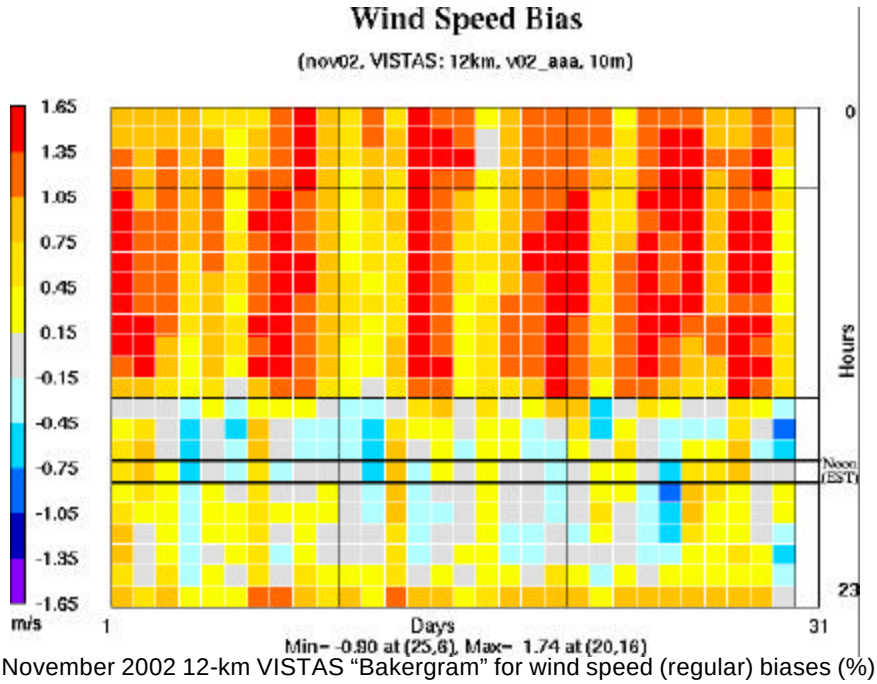


Figure 29. The November 2002 12-km VISTAS “Bakergram” for wind speed (regular) biases (%) is plotted. The hourly biases are shown in a calendar-like layout so that the upper left cell represents the 00Z bias on the first day of the month.

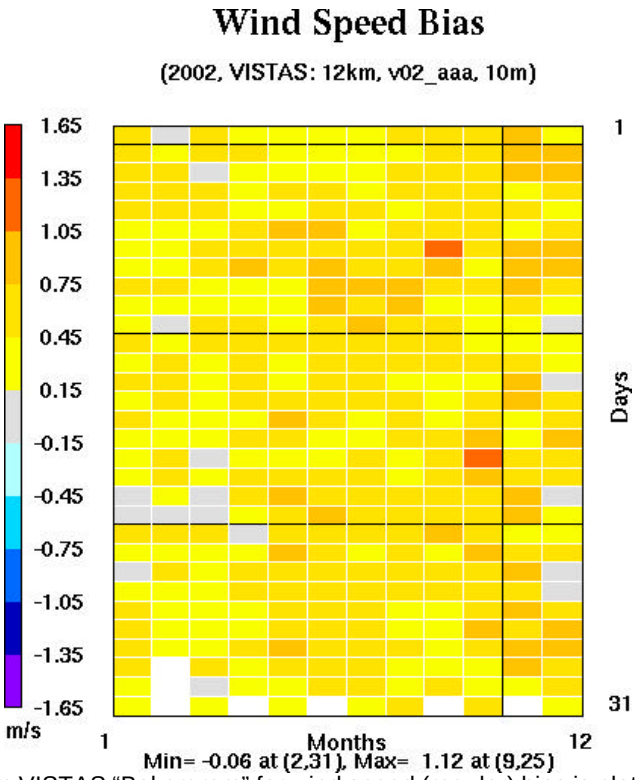


Figure 30. The 2002 12-km VISTAS "Bakergram" for wind speed (regular) bias is plotted. The data are shown in a calendar-like layout so that the upper left cell represents the bias on the first day of January.

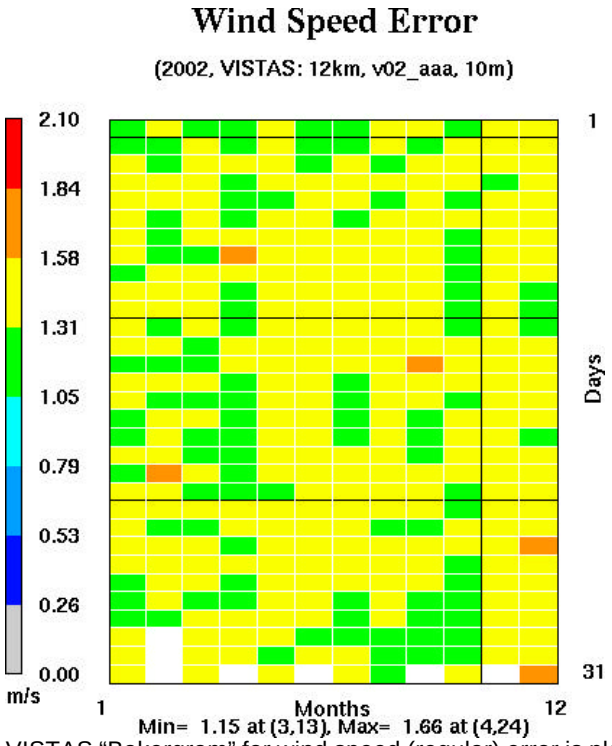


Figure 31. The 2002 12-km VISTAS "Bakergram" for wind speed (regular) error is plotted. The data are shown in a calendar-like layout so that the upper left cell represents the bias on the first day of January.

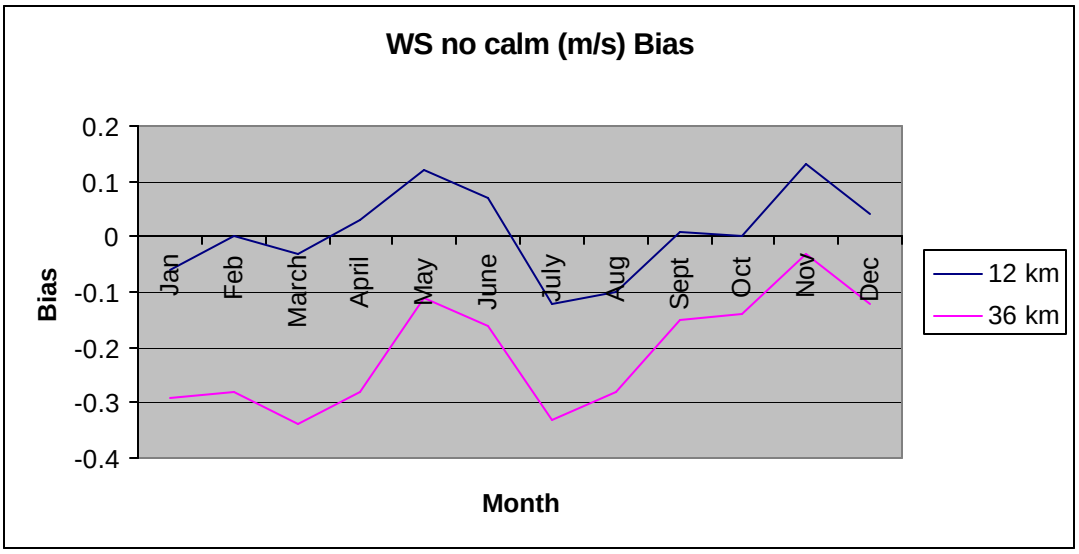


Figure 32. VISTAS region wind speed (no calms) biases (m/s) are plotted for both 12-km and 36-km resolutions.

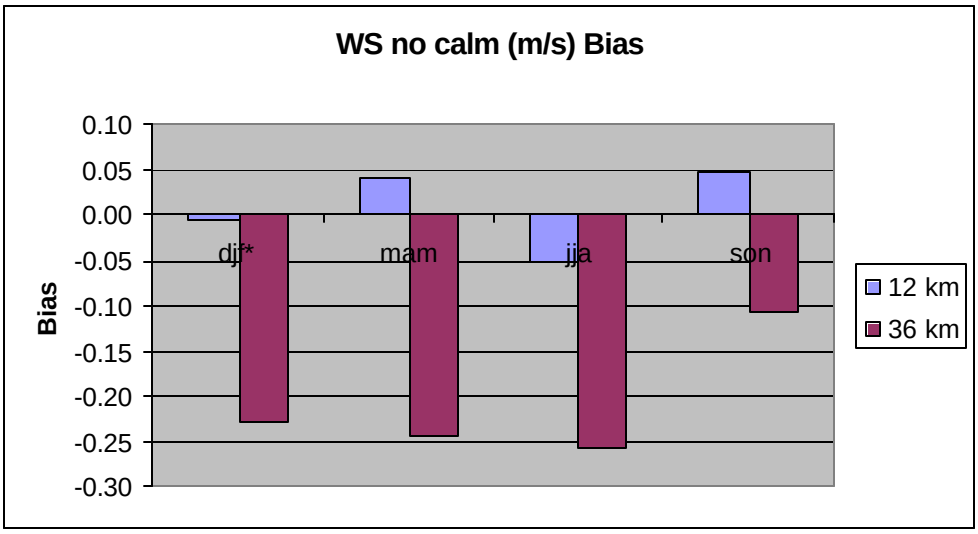


Figure 33. Seasonally aggregated VISTAS region wind speed (no calms) biases are shown for both the 36-km and 12-km grids.

* All months are in 2002, so the winter (djf) bar graph represents a discontinuous time period.

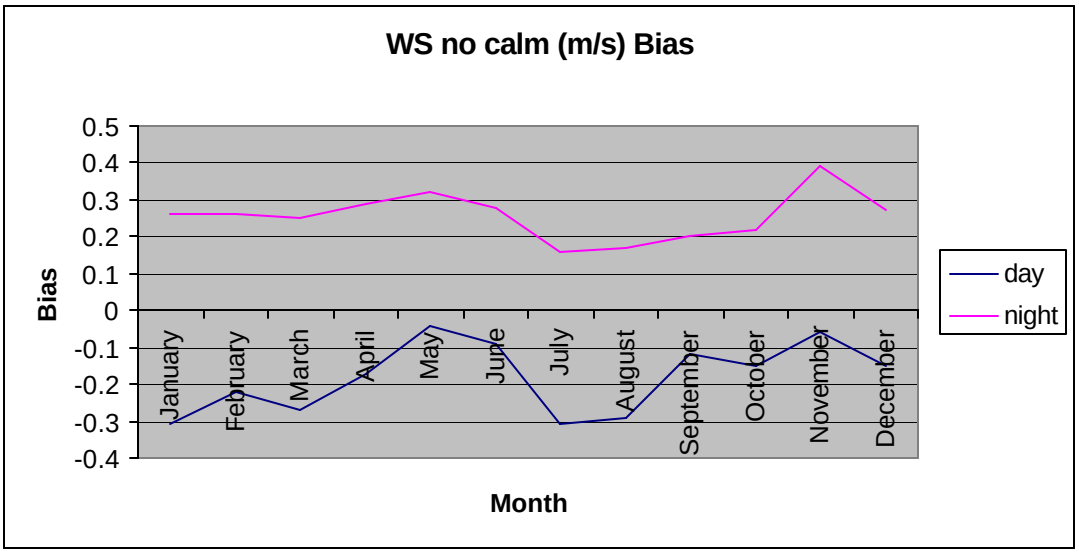


Figure 34. Monthly wind speed (no calms) biases for the 12-km VISTAS region are plotted. The “day” period is defined to be 12Z-23Z, while “night” is defined to be 00Z-11Z.

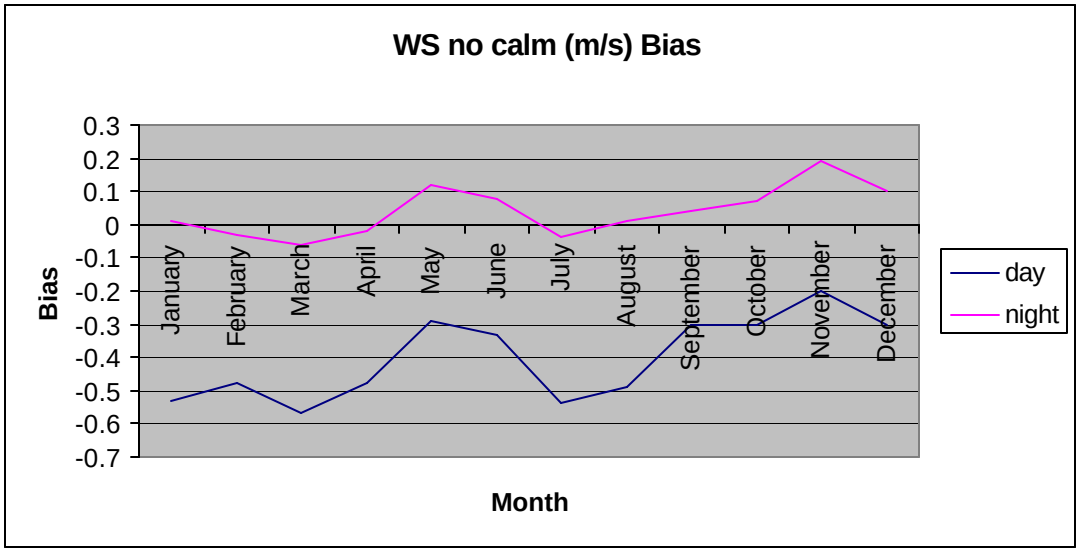


Figure 35. Monthly wind speed (no calms) biases for the 36-km VISTAS region are plotted. The “day” period is defined to be 12Z-23Z, while “night” is defined to be 00Z-11Z.

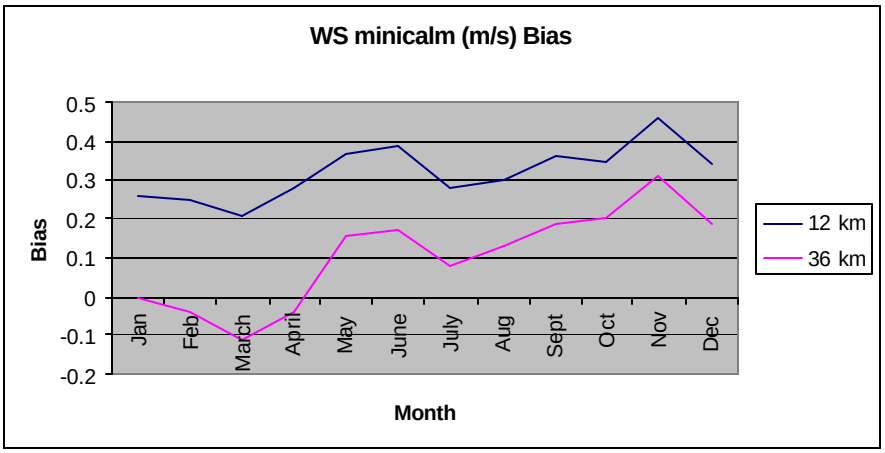


Figure 36. VISTAS region wind speed (minimum calms) biases (m/s) are plotted for both 12-km and 36-km resolutions.

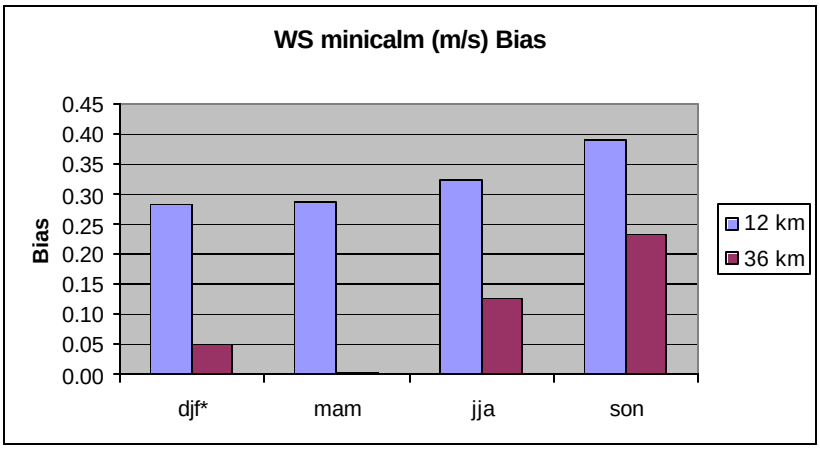


Figure 37. Seasonally aggregated VISTAS region wind speed (minimum calms) biases are shown for both the 36-km and 12-km grids.

* All months are in 2002, so the winter (djf) bar graph represents a discontinuous time period.

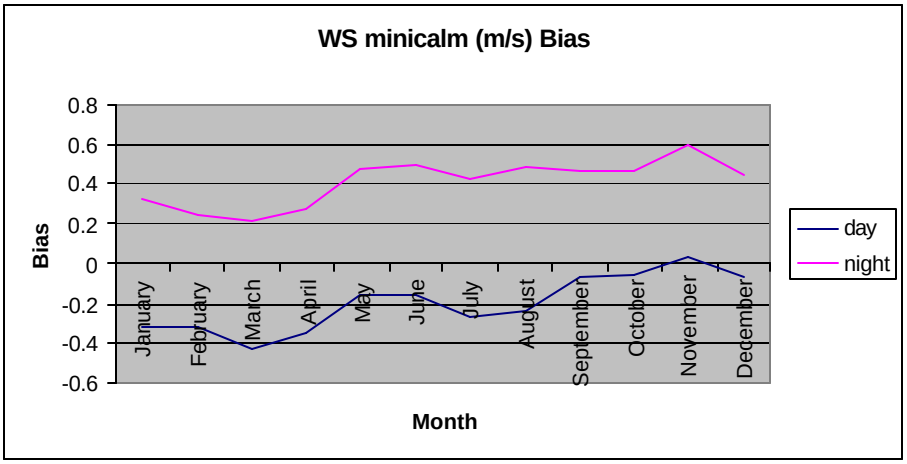


Figure 38. Monthly wind speed (minimum calms) biases for the 12-km VISTAS region are plotted. The "day" period is defined to be 12Z-23Z, while "night" is defined to be 00Z-11Z.

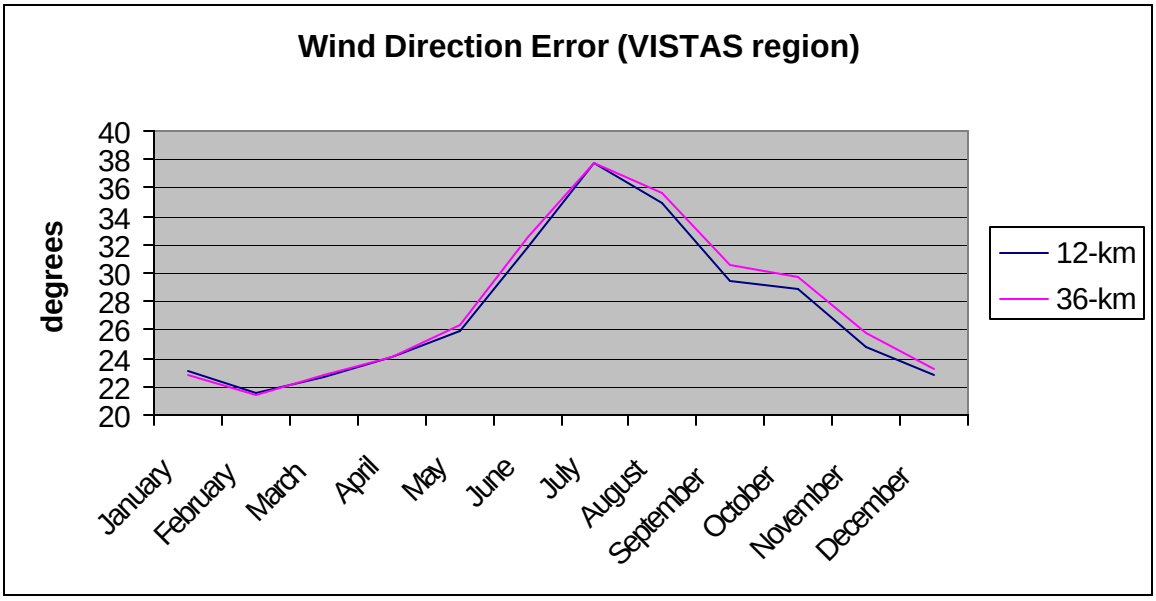


Figure 39. VISTAS region wind direction errors are plotted for both 12-km and 36-km resolutions.

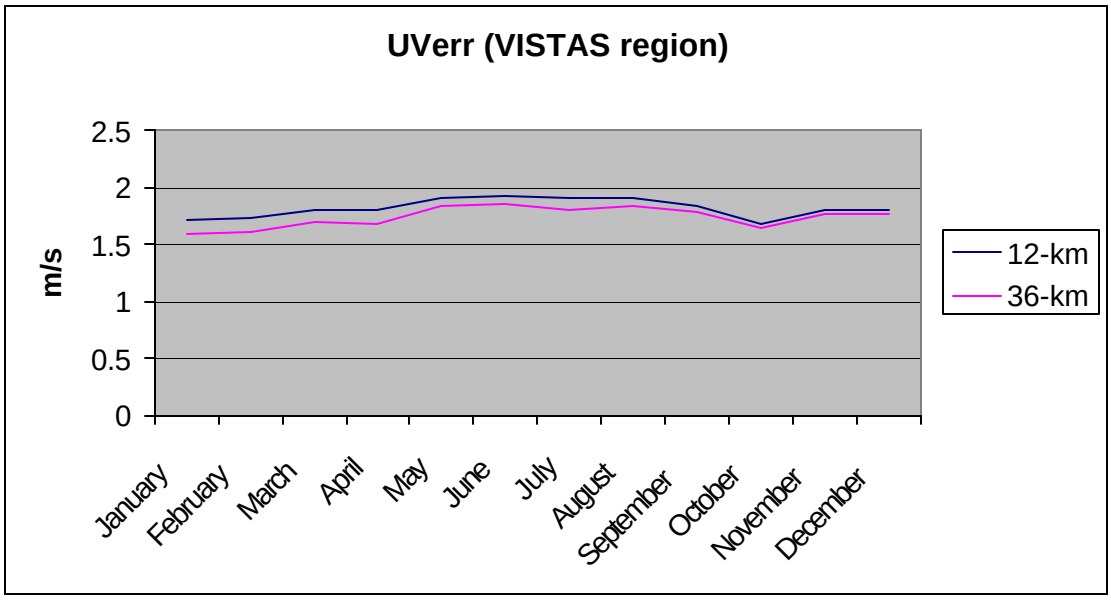


Figure 40. The magnitude of the error wind vector for the VISTAS region is plotted for both 12-km and 36-km resolutions.

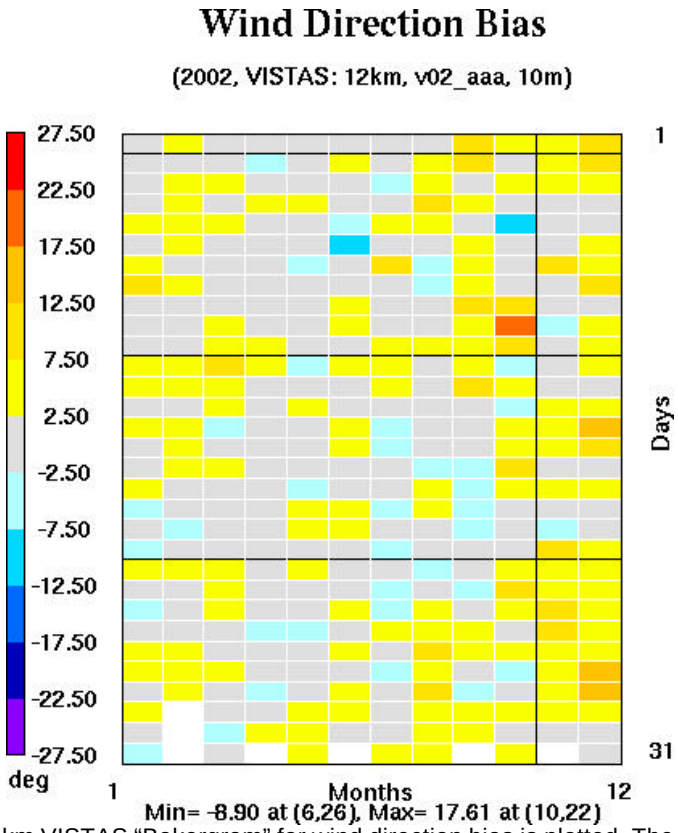


Figure 41. The 2002 12-km VISTAS "Bakergram" for wind direction bias is plotted. The data are shown in a calendar-like layout so that the upper left cell represents the bias on the first day of January.

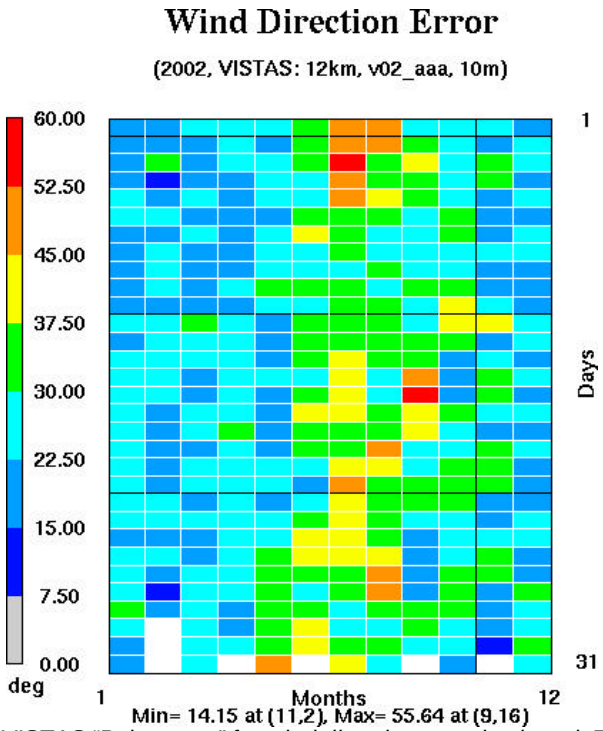


Figure 42. The 2002 12-km VISTAS "Bakergram" for wind direction error is plotted. The data are shown in a calendar-like layout so that the upper left cell represents the bias on the first day of January.

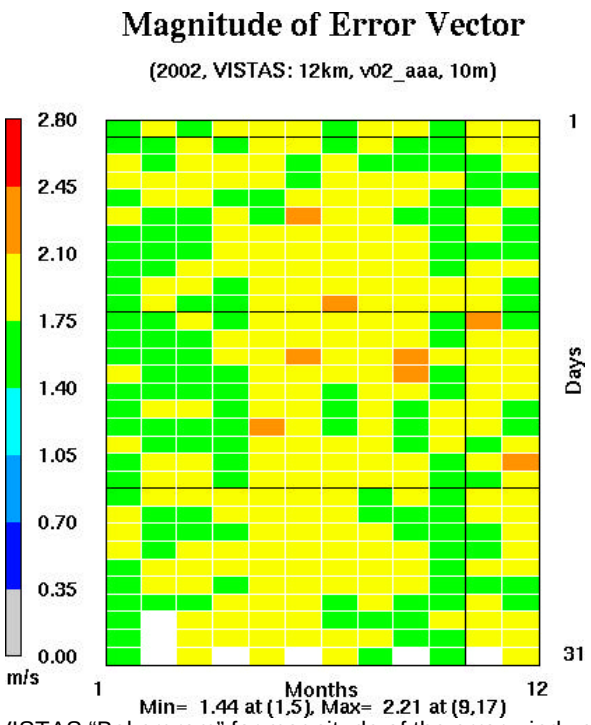


Figure 43. The 2002 12-km VISTAS "Bakergram" for magnitude of the error wind vector is plotted. The data are shown in a calendar-like layout so that the upper left cell represents the bias on the first day of January.

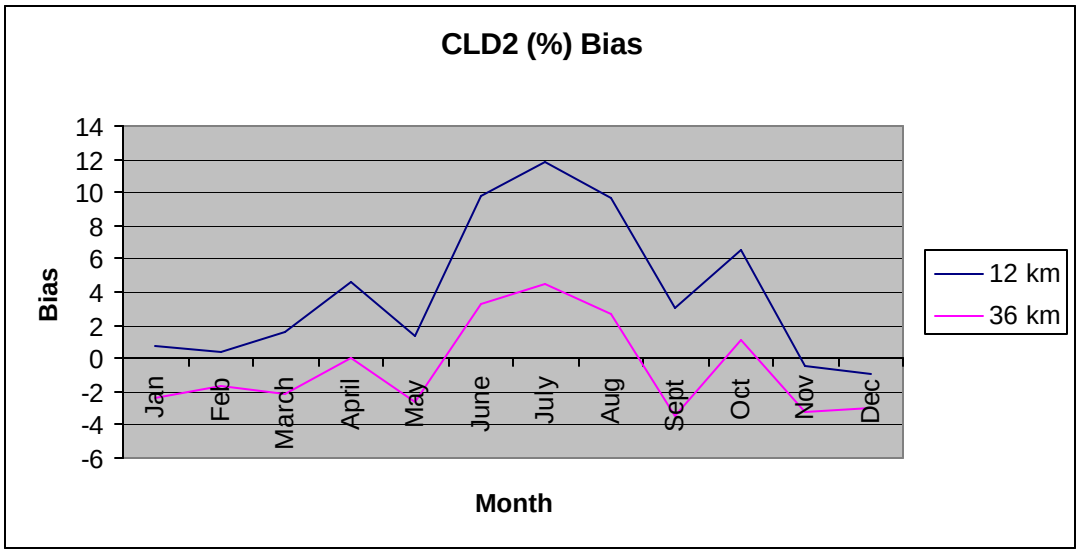


Figure 44. VISTAS region alternative cloud biases are plotted for both 12-km and 36-km resolutions.

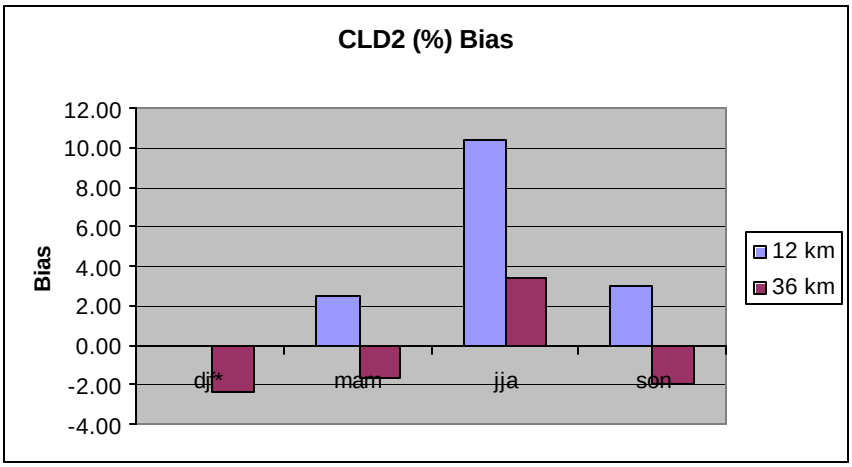


Figure 45. Seasonally aggregated VISTAS region alternative cloud biases are shown for both the 36-km and 12-km grids.

*All months are in 2002, so the winter (djf) bar graph represents a discontinuous time period.

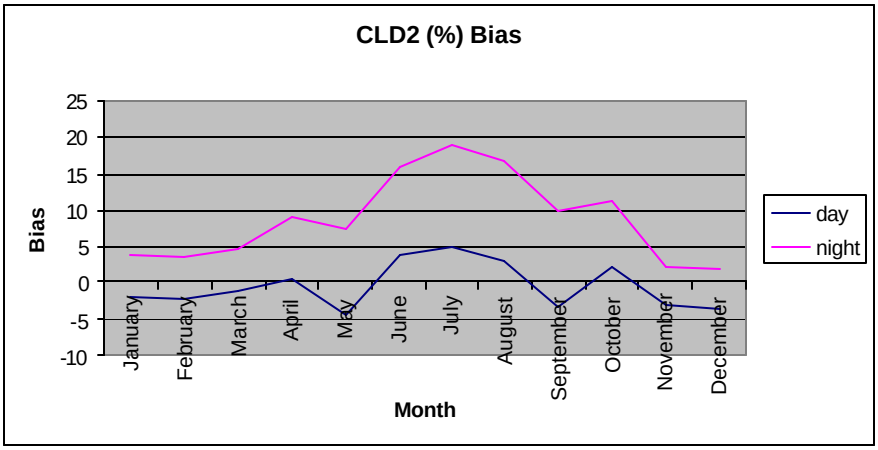


Figure 46. Monthly alternative cloud biases for the 12-km VISTAS region are plotted. The “day” period is defined to be 12Z-23Z, while “night” is defined to be 00Z-11Z.

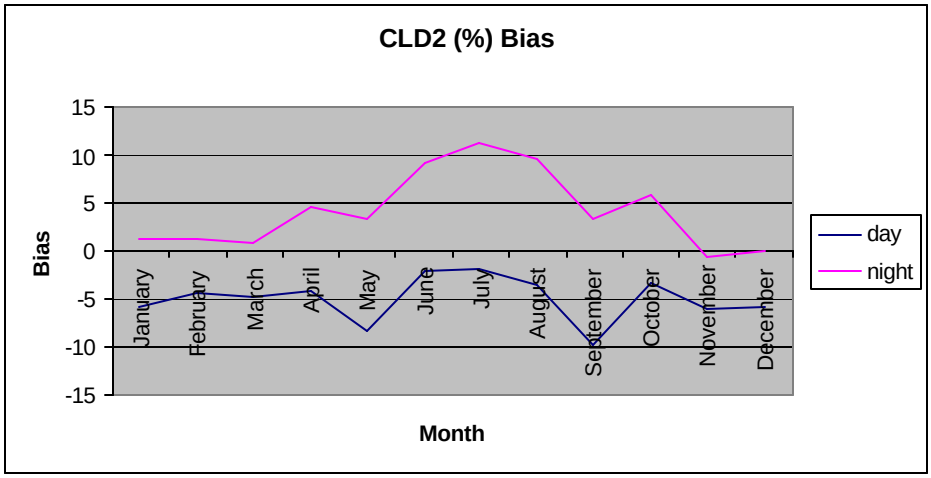


Figure 47. Monthly alternative cloud biases for the 36-km VISTAS region are plotted. The “day” period is defined to be 12Z-23Z, while “night” is defined to be 00Z-11Z.

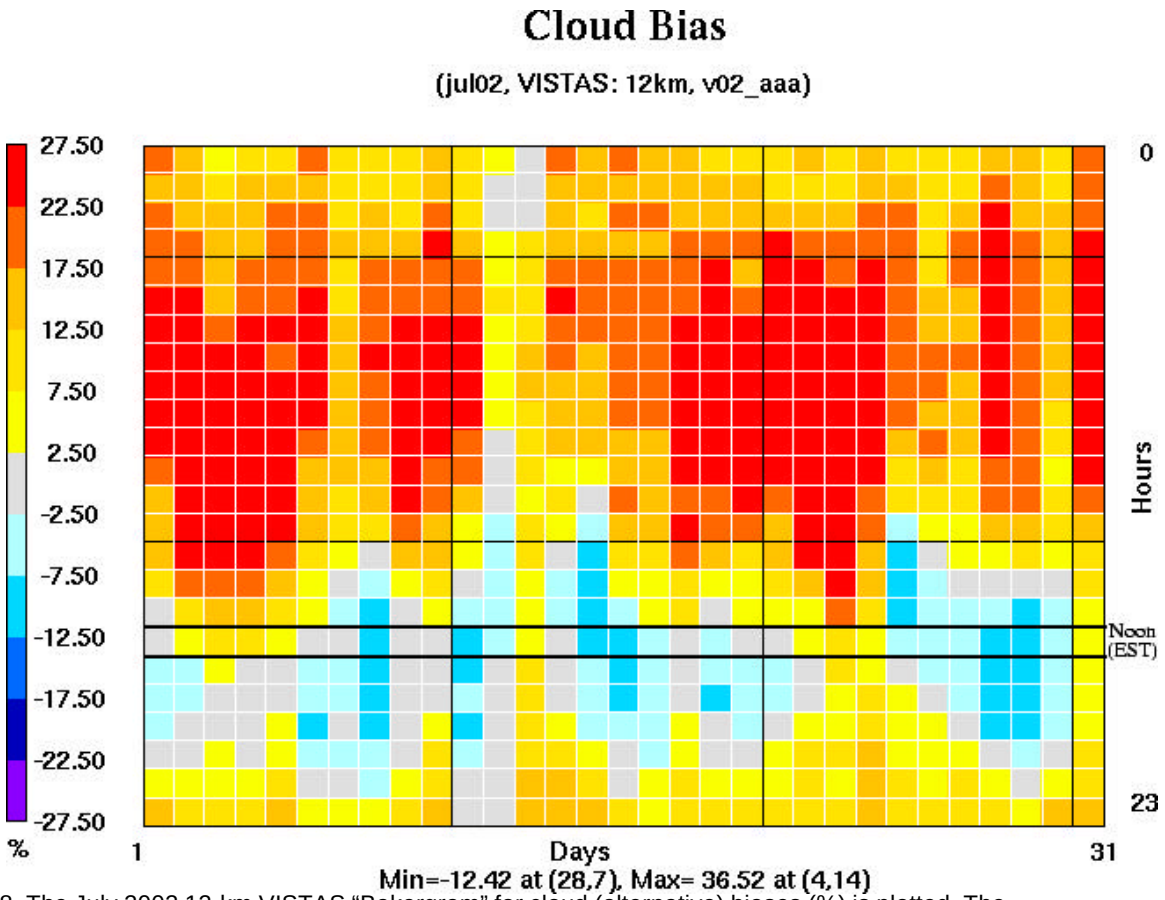


Figure 48. The July 2002 12-km VISTAS “Bakergram” for cloud (alternative) biases (%) is plotted. The hourly biases are shown in a calendar-like layout so that the upper left cell represents the 00Z bias on the first day of the month.

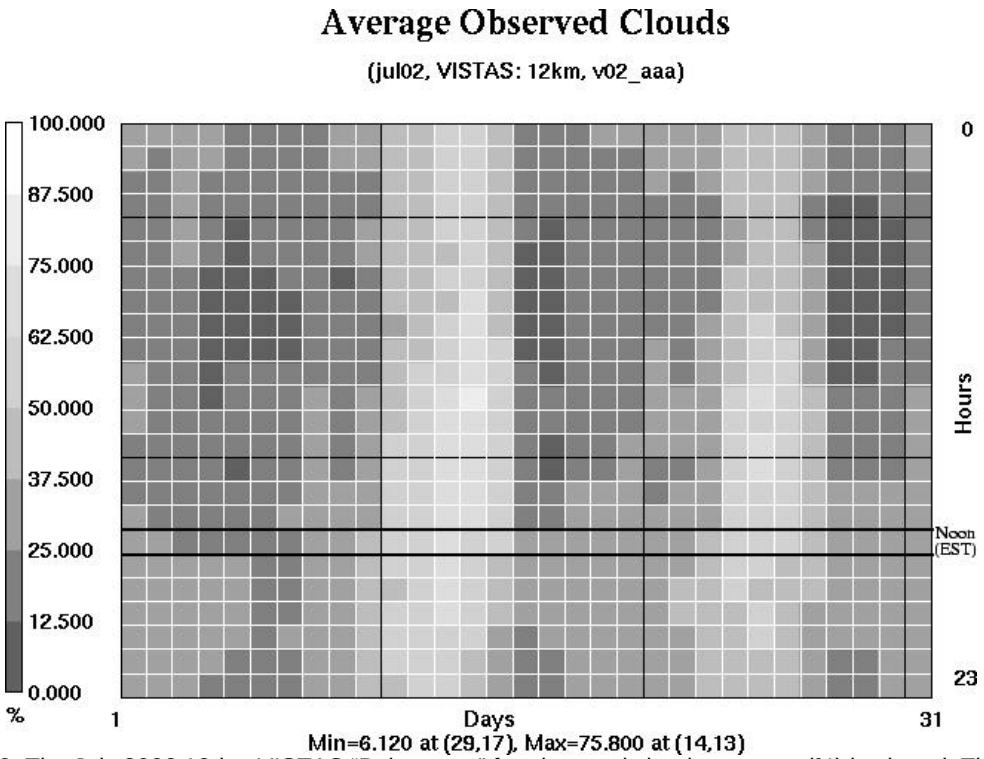


Figure 49. The July 2002 12-km VISTAS "Bakergram" for observed cloud coverage (%) is plotted. The hourly values are shown in a calendar-like layout so that the upper left cell represents the 00Z bias on the first day.

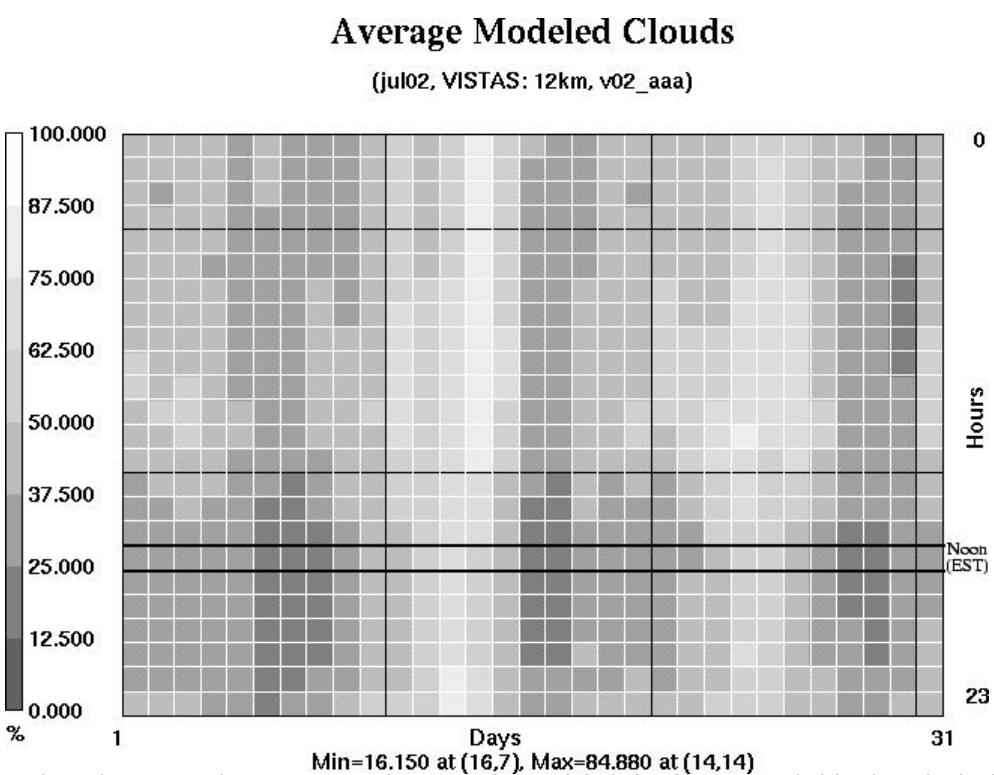


Figure 50. The July 2002 12-km VISTAS "Bakergram" for modeled cloud coverage (%) is plotted. The hourly values are shown in a calendar-like layout so that the upper left cell represents the 00Z bias on the first day.

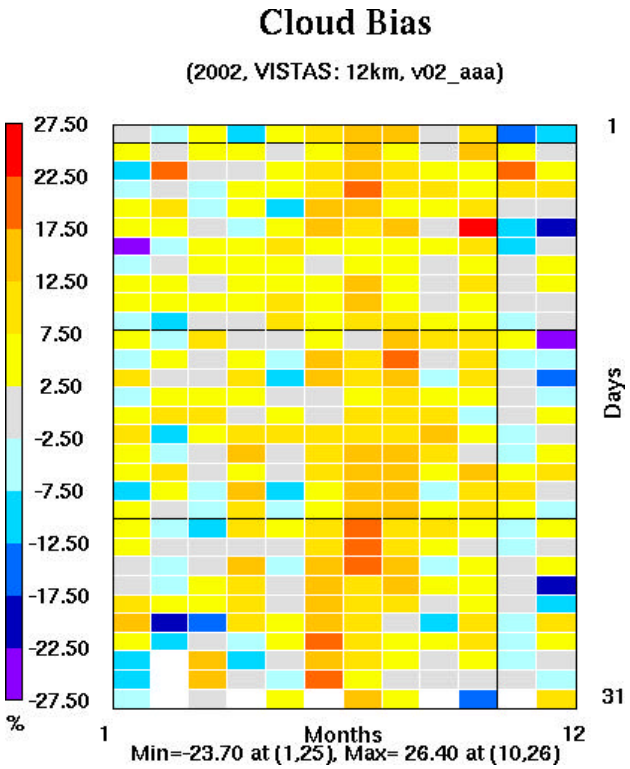


Figure 51. The 2002 12-km VISTAS "Bakergram" for cloud coverage (alternative) bias is plotted. The data are shown in a calendar-like layout so that the upper left cell represents the bias on the first day of January.

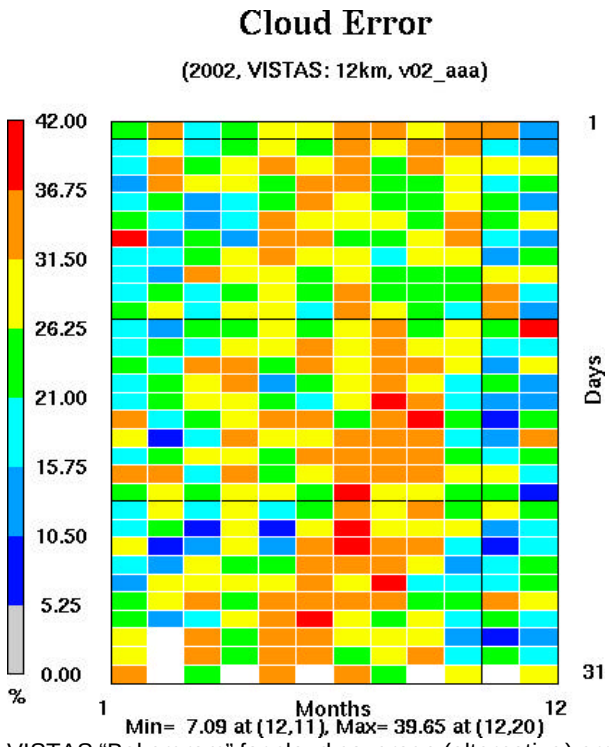


Figure 52. The 2002 12-km VISTAS "Bakergram" for cloud coverage (alternative) error is plotted. The data are shown in a calendar-like layout so that the upper left cell represents the bias on the first day of January.

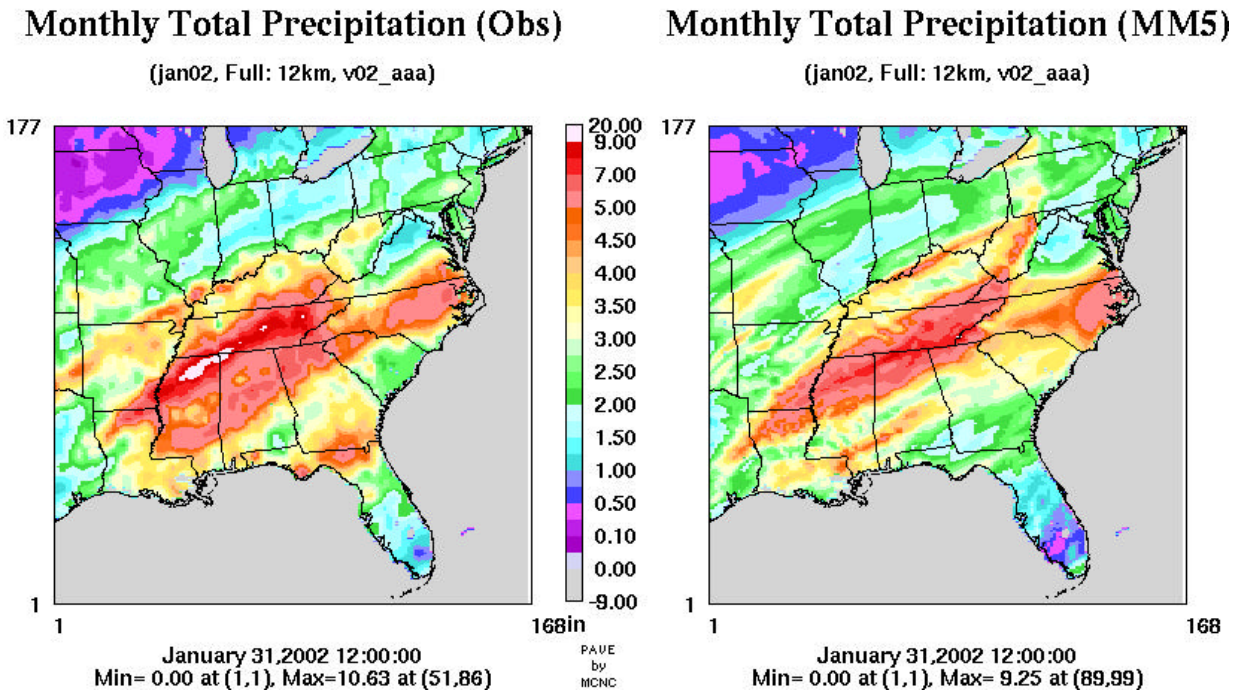


Figure 53. The January 2002 12-km accumulated precipitation from the Climate Prediction Center is juxtaposed with the MM5 accumulated precipitation.

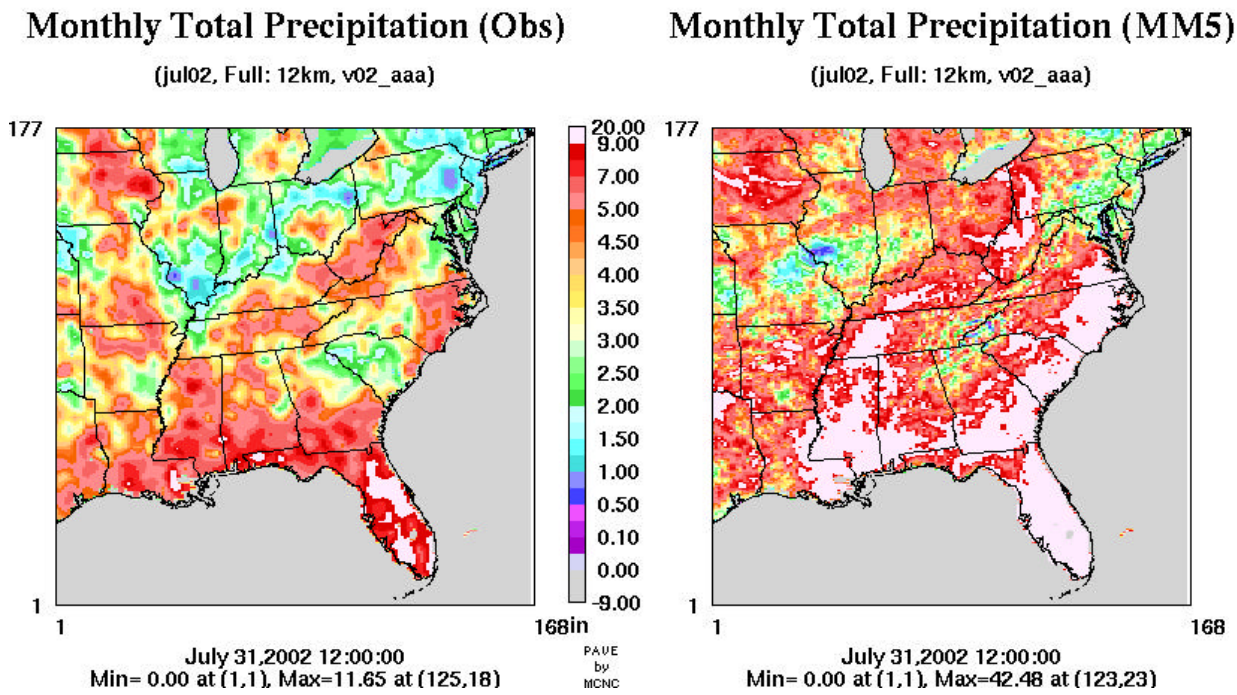


Figure 54. The July 2002 12-km accumulated precipitation from the Climate Prediction Center is juxtaposed with the MM5 accumulated precipitation.

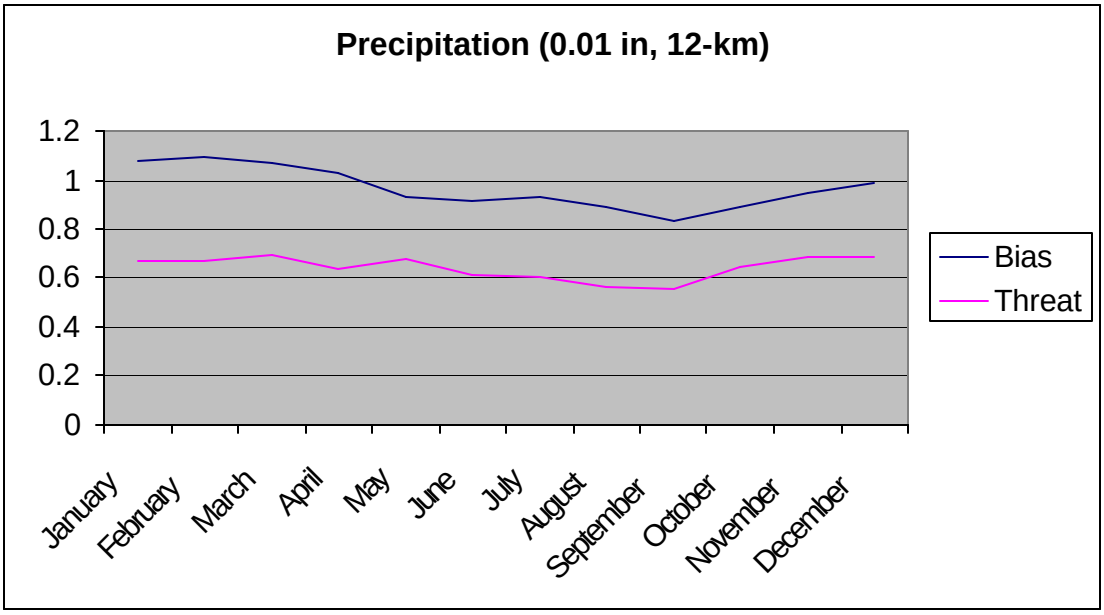


Figure 55. The 0.01 in threshold precipitation bias and threat score for the 12-km domain is shown for modeling year 2002.

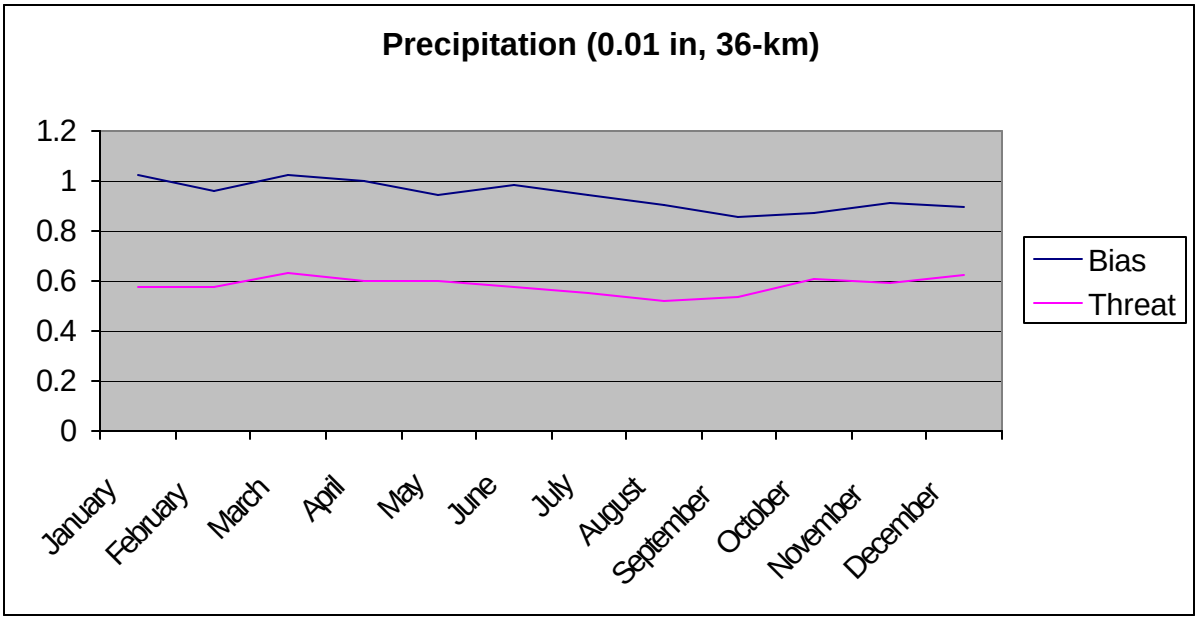


Figure 56. The 0.01 in threshold precipitation bias and threat score for the 36-km US region is shown for modeling year 2002.

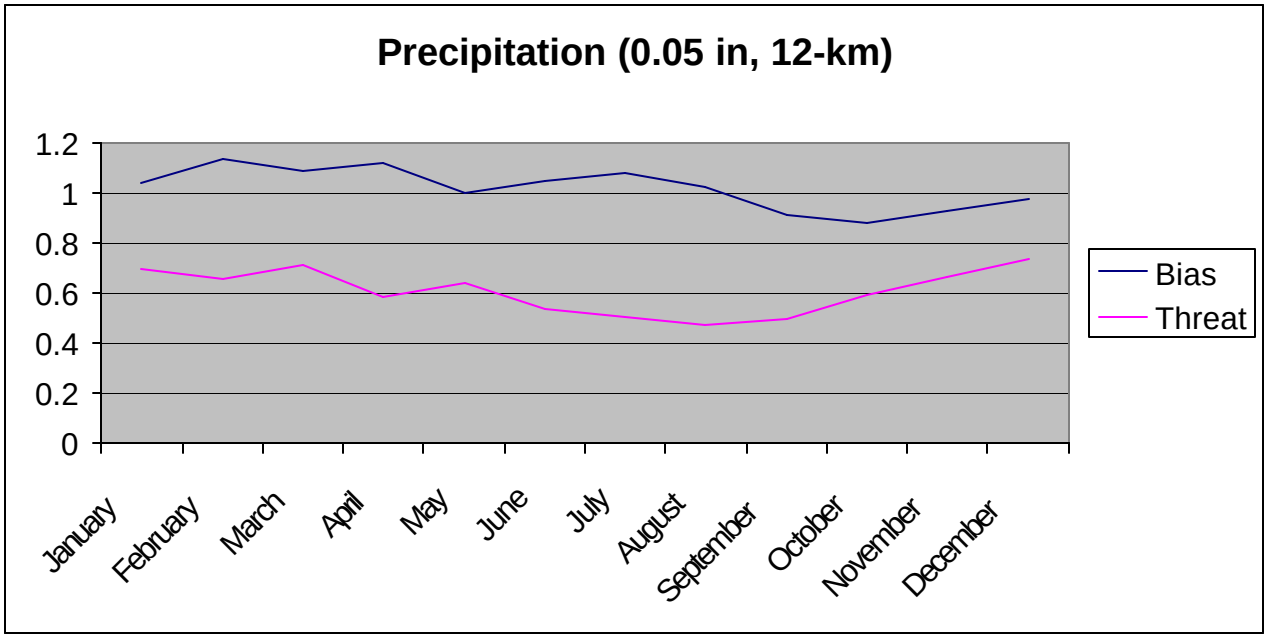


Figure 57. The 0.05 in threshold precipitation bias and threat score for the 12-km domain is shown for modeling year 2002.

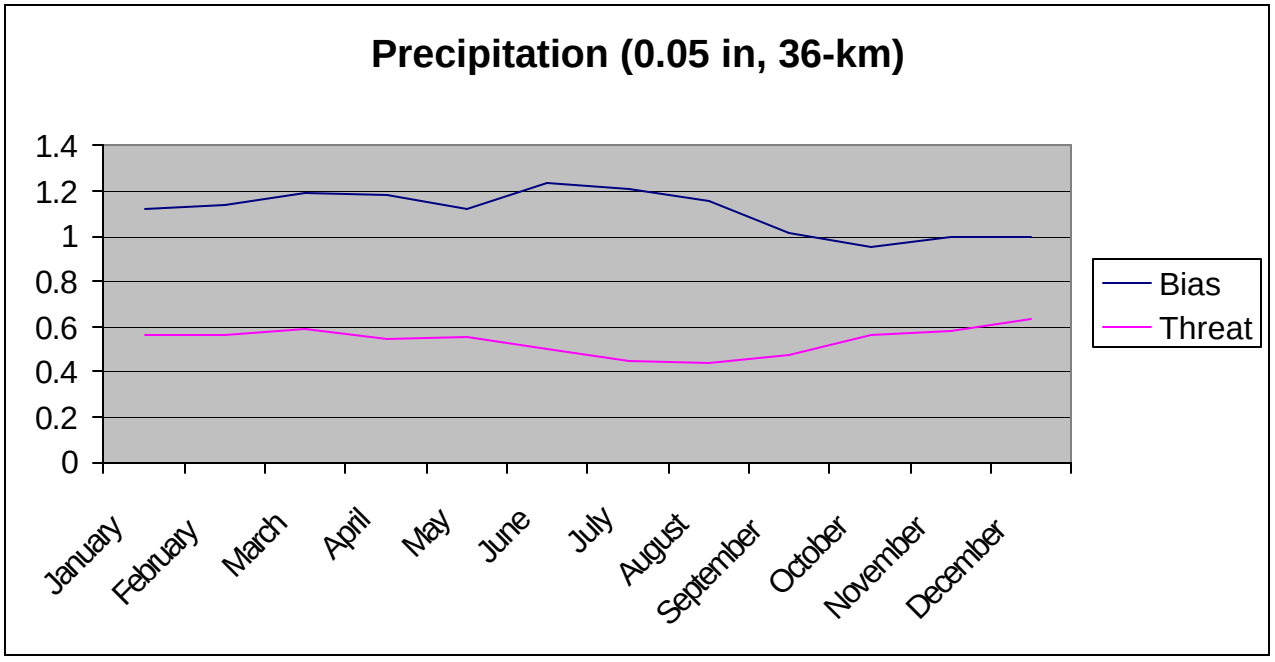


Figure 58. The 0.05 in threshold precipitation bias and threat score for the 36-km US region is shown for modeling year 2002.

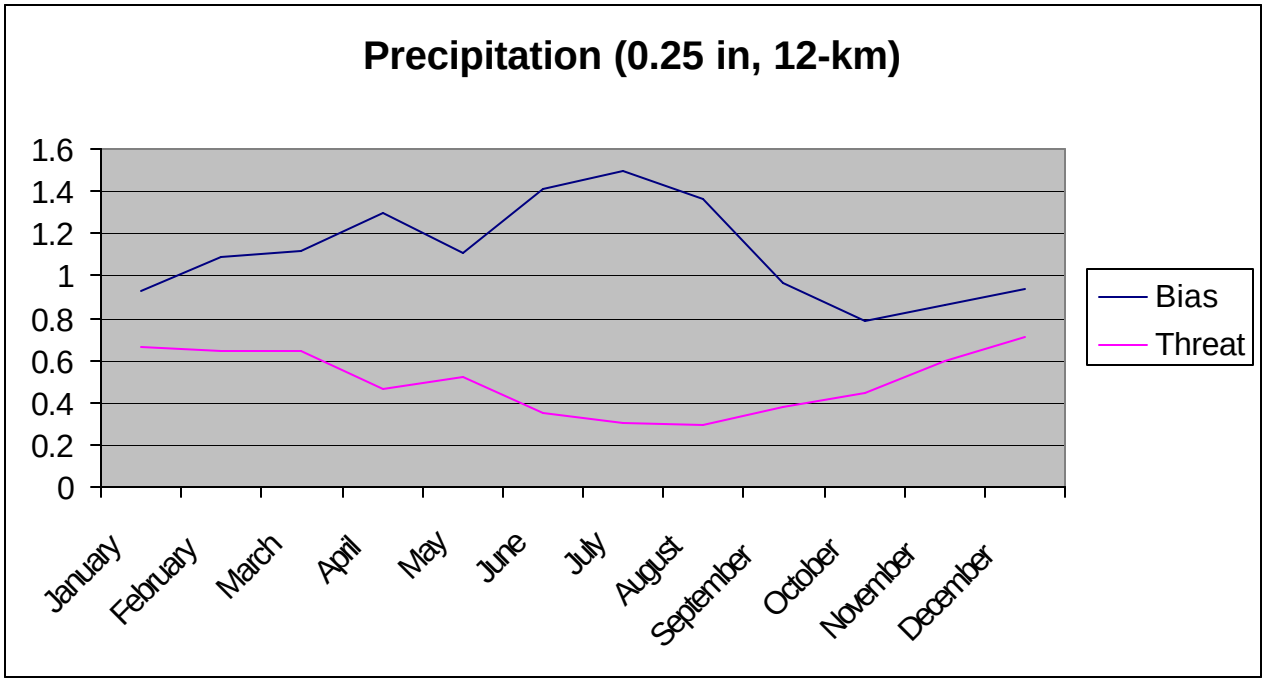


Figure 59. The 0.25 in threshold precipitation bias and threat score for the 12-km domain is shown for modeling year 2002.

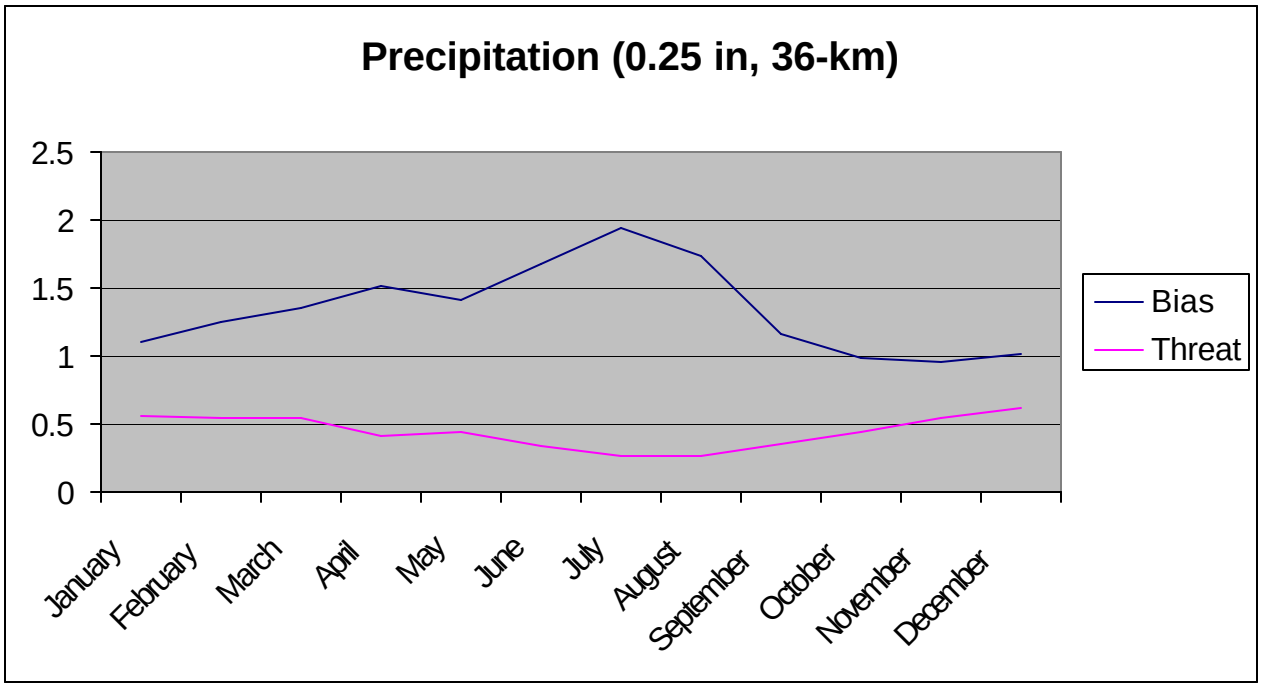


Figure 60. The 0.25 in threshold precipitation bias and threat score for the 36-km US region is shown for modeling year 2002.